doi:10.1006/jmbi.2001.5413 available online at http://www.idealibrary.com on IDEAL® J. Mol. Biol. (2002) 317, 21–40

JMB

Pre-steady-state and Stopped-flow Fluorescence Analysis of *Escherichia coli* Ribonuclease III: Insights into Mechanism and Conformational Changes Associated With Binding and Catalysis

Frank E. Campbell Jr[1]†, Adam G. Cassano[1]†, Vernon E. Anderson[2] and Michael E. Harris[1]*

[1]*Center for RNA Molecular Biology and*

[2]*Department of Biochemistry Case Western Reserve University School of Medicine Cleveland, OH 44106, USA*

To better understand substrate recognition and catalysis by RNase III, we examined steady-state and pre-steady-state reaction kinetics, and changes in intrinsic enzyme fluorescence. The multiple turnover cleavage of a model RNA substrate shows a pre-steady-state burst of product formation followed by a slower phase, indicating that the steady-state reaction rate is not limited by substrate cleavage. RNase III catalyzed hydrolysis is slower at low pH, permitting the use of pre-steady-state kinetics to measure the dissociation constant for formation of the enzyme-substrate complex ($K_d = 5.4(\pm 0.6)$ nM), and the rate constant for phosphodiester bond cleavage ($k_c = 1.160(\pm 0.001)$ min^{-1}, pH 5.4). Isotope incorporation analysis shows that a single solvent oxygen atom is incorporated into the 5′ phosphate of the RNA product, which demonstrates that the cleavage step is irreversible. Analysis of the pH dependence of the single turnover rate constant, k_c, fits best to a model for two or more titratable groups with pK_a of ca 5.6, suggesting a role for conserved acidic residues in catalysis. Additionally, we find that k_c is dependent on the pK_a value of the hydrated divalent metal ion included in the reaction, providing evidence for participation of a metal ion hydroxide in catalysis, potentially in developing the nucleophile for the hydrolysis reaction. In order to assess whether conformational changes also contribute to the enzyme mechanism, we monitored intrinsic tryptophan fluorescence. During a single round of binding and cleavage by the enzyme we detect a biphasic change in fluorescence. The rate of the initial increase in fluorescence was dependent on substrate concentration yielding a second-order rate constant of $1.0(\pm 0.1) \times 10^8$ M^{-1} s^{-1}, while the rate constant of the second phase was concentration independent ($6.4(\pm 0.8)$ s^{-1}; pH 7.3). These data, together with the unique dependence of each phase on divalent metal ion identity and pH, support the hypothesis that the two fluorescence transitions, which we attribute to conformational changes, correlate with substrate binding and catalysis.

Keywords: ribonuclease III; endonuclease; phosphodiesterase; enzyme kinetics; stopped-flow fluorescence

*Corresponding author

Introduction

The enzyme ribonuclease III (EC 3.1.26.3) was the first specific ribonuclease to be discovered and purified.[1] Although at the time the enzyme's role in cell function was unclear, it has since been shown that RNase III plays multiple roles in RNA processing and gene expression by recognizing different RNA substrates.[2] The participation of

†These two authors contributed equally to this work.

Abbreviations used: dsRBD, double-stranded RNA binding domain; RRM, RNA recognition motif.

E-mail address of the corresponding author: meh2@pop.cwru.edu

0022-2836/02/010021–20 $35.00/0

RNase III in numerous aspects of RNA metabolism and the general features of substrate binding are well established; however, a detailed understanding of the mechanisms of molecular recognition and catalysis by *Escherichia coli* RNase III, the archetypical example of this class of enzyme, is lacking.

A hallmark of RNase III is its involvement in the processing of multiple cellular RNAs. RNase III plays an important role in rRNA processing by cleaving both strands of duplex RNA formed by base-pairing between the 5′ and 3′ sequences flanking the mature rRNA sequences, generating the immediate precursors to 16 S and 23 S rRNAs.[3,4] Additionally, RNase III removes some bacterial rRNA introns, producing the fragmented rRNAs of *Rhodobacter capsulatus* and *Salmonella typhimurium*.[5] The enzyme also recognizes additional, non-ribosomal RNA substrates *in vivo*, including specific mRNAs from *E. coli*, and bacteriophages λ and T7,[2] where cleavage is linked to regulation of gene expression.[6,7] In eukaryotes, RNase III is involved in the maturation of U2 and U5 small nuclear RNAs, and a large subset of small nucleolar RNAs,[8,9] in addition to its function in rRNA processing.[10] Recently, a protein containing sequence motifs found in all RNase III enzymes was shown to participate in the initial step of gene silencing by RNA interference.[11] Thus, detailed analysis of the kinetic and enzymatic behavior of bacterial RNase III will have general significance for this broad family of enzymes.

E. coli RNase III is a homodimer of a 226 amino acid (26 kDa) polypeptide, and like most proteins that interact with RNA, the enzyme appears to be composed of multiple functional domains. The amino acid sequence of the monomer suggests a folded protein consisting of two domains. The C-terminal domain consists of a single ca 70 amino acid residue double-stranded RNA binding domain (dsRBD).[12,13] The larger N-terminal domain is thought to contain at least a portion of the monomer active site as well as the dimer interface. Sequence alignment of RNase III orthologues identifies a collection of conserved amino acids including several acidic residues in the N-terminal domain,[14] that are believed to be involved in formation of the enzyme active site.

RNase III usually, but not always, cleaves within double-stranded RNA leaving a two-nucleotide 3′ overhang.[2] Inspection of the secondary structures of *E. coli* RNase III substrates indicates that strand cleavage sites are flanked by 10-14 nucleotides of base-paired sequence resulting in a 20-30 nucleotide double helical substrate. Deletion studies are consistent with a role for helical structure in substrate recognition,[15] but most *in vivo* substrates have more complex structures. Alignment of ca 70 known RNase III cleavage sites reveals weakly conserved sequence motifs adjacent to sites of cleavage.[16] However, substrates can deviate significantly from the consensus, yet are apparently recognized efficiently *in vivo*, and mutations within these sequences had little effect on multiple turnover cleavage of a model substrate by RNase III.[17] Interestingly, a re-examination of the sequence data revealed an exclusion of certain sequences at defined positions relative to the cleavage site; inclusion of these ''disfavored'' sequences in a model substrate inhibited binding.[18] Thus, exclusion of non-cognate RNAs appears to be an important aspect of substrate recognition; however, the precise interactions between RNase III and its substrates are not well understood. Clearly, a detailed understanding of the kinetics and thermodynamics of recognition by RNase III will be essential for understanding discrimination between cognate and non-cognate RNAs.

Biochemical and structural studies of RNA-protein interactions over the past decade revealed that recognition is most often accompanied by conformational changes coupled to formation of specific complexes; however, the functional significance of this dynamic behavior has only been defined in a few instances.[19–21] Issues of conformational dynamics appear to be particularly relevant for dsRBD-containing proteins such as RNase III. Bevilacqua and colleagues recently showed that dsRBD binding induces a more *A*-form helical geometry in RNAs containing internal bulges.[22] Given that most RNase III substrates *in vivo* also have irregular structures, it is relevant to ask whether corresponding conformational changes involving the dsRBD occur in substrate recognition by RNase III. The importance of this issue is underscored by evidence that changes in enzyme conformation are coupled to specificity in other enzymes that recognize complex macromolecular substrates such as amino-acyl tRNA synthetases and restriction enzymes.[23–25]

RNase III catalyzes the hydrolysis of the P-3′O phosphodiester bond in RNA generating 5′ phosphate and 3′ hydroxyl termini, and requires divalent metal ion(s) for activity.[26] Thus, RNase III belongs to a broad class of phosphodiesterase enzymes, including large ribozymes, polymerases and restriction endonucleases, that use active site metal ions for catalysis of phosphoryl transfer reactions.[27] Based on structural and kinetic evidence, models for catalysis by these enzymes that involve one or more active site metal ions have been proposed.[27,28] A mechanism with two ions coordinated to the reactive phosphoryl can be used to describe the general features of metal ion dependent phosphodiesterase catalysis. Here, one ion coordinates to the bridging oxygen atom of the leaving group while the second interacts with the attacking nucleophile.[29] Although the ''two metal ion'' mechanism appears to hold for the polymerase-derived exonucleases such as Klenow,[30] and has provided a useful framework for exploring mechanisms of enzymatic phosphoryl transfer, there is evidence that only a single metal ion is required for catalysis by some phosphodiesterases.[31,32] Additionally, recent analyses of group I ribozyme catalysis indicate that at least

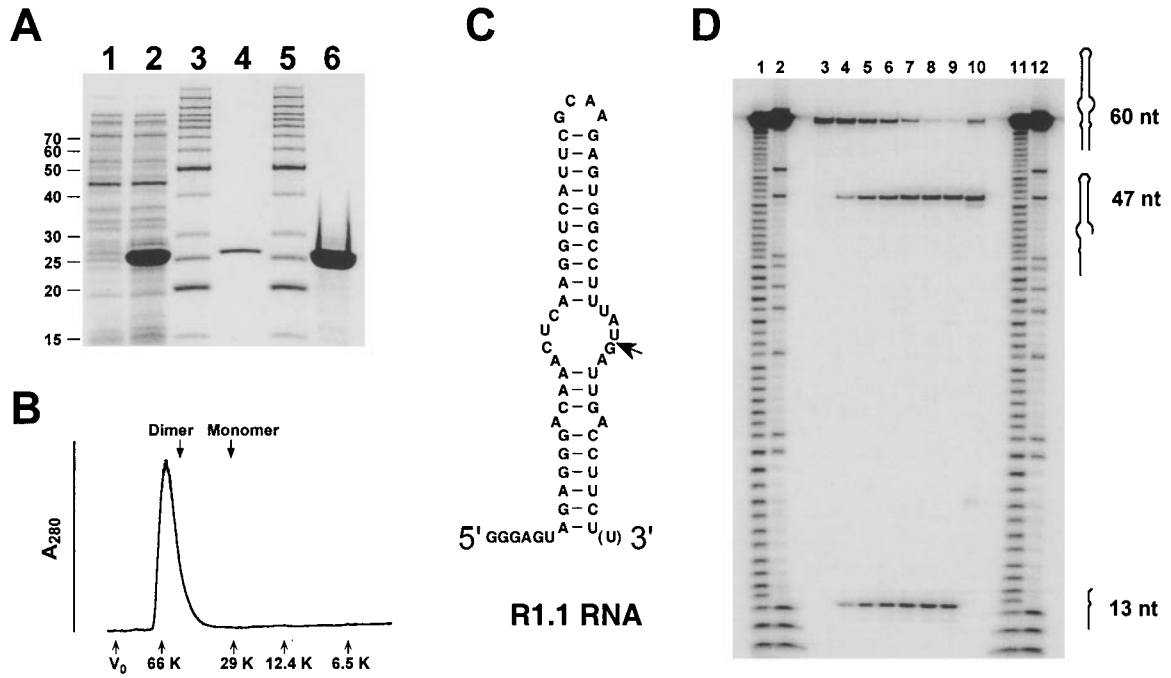

Figure 1. Purification and analysis of *E. coli* RNase III. (a) Analysis of purified RNase III enzyme by SDS-PAGE. Lane 1, whole cell lysate taken prior to induction; lane 2, whole cell lysate taken four hours after induction with IPTG; lanes 3 and 5, Benchmark protein size standards (Gibco-BRL); lanes 4 and 6, 1 μg and 20 μg, respectively, of the final purified RNase III preparation. (b) Analysis of the dimerization state of RNase III by gel-filtration chromatography. The V_e values for a series of molecular mass standards and the void volume, V_0 are indicated. The notation of ''dimer'' and ''monomer'' indicate the positions at which material of 52 kDa and 26 kDa, respectively, would be predicted to elute based on a standard curve obtained from the V_e values shown. The elution peak observed for the RNase III sample corresponds to an apparent molecular mass of 62 kDa. (c) Secondary structure of the R1.1 RNA substrate. The primary cleavage site is indicated by an arrow. (d) Specificity of RNase III cleavage and visualization of reaction products. RNase III cleavage reactions were performed under pre-steady-state conditions at pH 5.4 with 5 nM R1.1 RNA and 2 μM RNase III. The reactions corresponding to lanes 3 through 9 contained uniformly labeled substrate, while the reaction of lane 10, as well as the markers in lanes 1, 2, 11, and 12 utilized (5′-^{32}P) end-labeled R1.1 RNA. The reaction in lane 3 contained no RNase III, and was incubated for one hour at 37 °C. Lanes 4-9 correspond to aliquots taken from a single reaction after 10, 30, 50, 90 seconds, five minutes and one hour. The reaction containing end-labeled RNA in lane 10 was also incubated for one hour. Lanes 1 and 11 correspond to partial alkaline hydrolysis of end-labeled R1.1 RNA, and lanes 2 and 12 show partial ribonuclease T_1 digests of the same material. The position and size of the precursor substrate (60 nt), the 5′ cleavage product (47 nt) and the 3′ cleavage product (13 nt) are indicated.

three distinct metal ions interact with the reactive phosphoryl,[33] and protein enzymes with as many active site metals have also been described.[34]

The importance of magnesium (Mg^{2+}) ions in RNase III catalysis is well established, and recent evidence also supports a role for metal ions in stabilizing the enzyme-substrate complex.[35] Interestingly, the specificity of metal ion participation in binding differs from those metal ion binding sites important for catalysis, since calcium (Ca^{2+}) supports binding, but not catalysis. Evidence for the participation of specific RNase III residues in metal ion interactions comes from the observation that mutation of one of the conserved acidic residues within the catalytic domain (Glu117) results in an enzyme that can bind substrate, but promotes catalysis at a greatly reduced rate.[35] The deleterious effects of an aspartic acid substitution at Glu117 can be somewhat ameliorated by the presence of manganese (Mn^{2+}), and this mutant enzyme is less susceptible to inhibition by high concentrations of Mn^{2+}.[36] Thus, it appears that, like other metal dependent phosphodiesterases,[27] acidic residues may play a role in positioning metal ions involved in RNase III function. However, the number and affinity of metal ions required for binding and catalysis, the roles they play in catalytic mechanism, and the enzyme residues involved in metal ion interactions are not well defined.

A fundamental impediment to understanding the mechanisms of recognition and catalysis by RNase III is that it is not known whether modifications in enzyme or substrate structure that have thus far been examined directly affect substrate recognition, catalysis, or some other aspect of the reaction pathway. Importantly, the contributions of conformational changes, which can complicate the interpretation of structure-function studies,[37] have

not been assessed. To address these issues and to provide a context for exploring the molecular mechanisms of substrate recognition and catalysis, we examined the steady-state and pre-steady-state reaction kinetics of RNase III cleavage of a commonly used model substrate. Here we provide evidence that the steady-state cleavage rate does not directly reflect substrate cleavage, but rather is limited by a slow step subsequent to catalysis. Pre-steady-state reaction kinetics, however, provide a means for directly monitoring both substrate binding and catalysis. This framework permitted several insights into the RNase III reaction mechanism, including an assessment of the number of acidic residues involved in catalysis and evidence for the participation of a metal hydroxide in the transition state. Furthermore, stopped-flow fluorescence studies revealed conformational changes associated with both binding and catalysis by RNase III. Together, the results provide significant new insight into the kinetic and dynamic features of substrate recognition and catalysis by *E. coli* RNase III.

Results

Analysis of steady-state reaction kinetics

RNase III was over-produced in *E. coli* and purified as described.[26,38,39] The purified material has mobility corresponding to the expected molecular mass of 26 kDa with few additional proteins (<1-2%) detected by Coomassie blue staining (Figure 1(a)). Further analysis of the enzyme preparation by gel-filtration chromatography demonstrates that all purified enzyme is in the dimeric form (Figure 1(b)). R1.1 RNA, a well-characterized model substrate derived from bacteriophage T7 was utilized in our analysis (Figure 1(c)). Under relatively low (150 mM KCl) monovalent ion conditions, RNase III cleaves a single phosphodiester bond in the 60 nt RNA generating a 47 nt 5′ fragment and a 13 nt 3′ fragment.[40] Figure 1(d) shows separation by denaturing gel electrophoresis of precursor and product RNA fragments in samples from a time course of RNase III cleavage of uniformly radiolabeled R1.1 RNA. Comparison of the cleavage products obtained using uniformly labeled and 5′ end-labeled R1.1 RNA identifies the 47 nt fragment as the 5′ cleavage product (Figure 1(d)). The mobility of this fragment relative to partial digests generated using hydroxide and RNase T_1 is consistent with cleavage at the correct phosphodiester bond. Importantly, these data demonstrate that quantification of the time and enzyme-dependent generation of accurately cleaved products is not complicated by secondary cleavages, or by contaminating endonucleases in the enzyme preparation.

First, we determined the steady-state kinetic parameters k_{cat} and K_m for the multiple turnover cleavage of the R1.1 substrate by RNase III. Multiple turnover reactions were performed over a range of

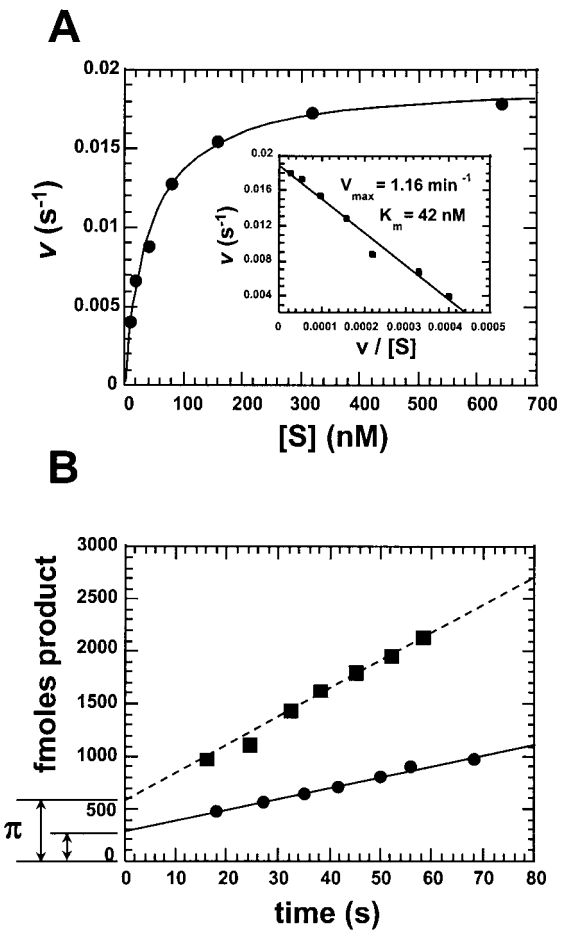

Figure 2. Steady-state kinetic analysis of R1.1 RNA cleavage at neutral pH. (a) Dependence of the initial rate on substrate concentration. Representative data for multiple turnover reactions performed at pH 7.5 (Tris-HCl) using (5′-^{32}P) end-labeled R1.1 substrate are shown. Substrate concentrations were varied from 10 nM to 640 nM and enzyme concentration varied from 62.5 pM to 4 nM, maintaining [S]/[E>] $\geqslant$ 40 and keeping the fraction cut in each reaction under 10%. The duration of each time-course varied from two minutes to 100 minutes depending on the enzyme concentration. Rates at each substrate concentration were determined by a linear fit of the fraction substrate consumed *versus* time. The data are fit to the Michaelis-Menton equation; $v = V_{max}/(1 + (K_m/[S]))$. The inset shows the same data plotted as v *versus* $v/[S]$ (Eadie-Hofstee) and fit to $v = V_{max} - K_m$ $(v/[S])$. Both plots provide equivalent values for V_{max} and K_m ($V_{max} = 1.16$ min^{-1} and $K_m = 42$ nM). (b) Analysis of the magnitude of the apparent pre-steady-state burst. A plot of moles of product formed *versus* time is shown for multiple turnover reactions performed at pH 8.0 (Tris-HCl) using (5′-^{32}P) end-labeled R1.1 substrate. The data are fit to a linear equation and extrapolated to the y axis. The amplitude of the burst (π) is shown at the left. Squares indicate data from a reaction containing 40 nM RNase III and 200 nM R1.1 RNA; circles depict data from a reaction containing 20 nM RNase III and 100 nM R1.1 RNA. The ratio of the y-intercepts is 2.

substrate concentrations, and for each, the plots of product accumulation *versus* time were fit to a linear equation. Figure 2(a) shows a plot of these initial rates *versus* substrate concentration from cleavage reactions containing 10-640 nM R1.1 RNA. The data fit well to both hyperbolic and linearized (Eadie-Hoftsee) versions of the Michaelis-Menten equation and give a k_{cat} value of 1.16 min^{-1} and K_m of 42 nM. These measurements differ somewhat from values of 3.8 min^{-1} for k_{cat}, and 335 nM for K_m that were recently reported using the R1.1 substrate.[36] One source of this difference could arise from the manner in which the reactions are performed, since in the present case reactions were initiated by mixing enzyme and substrate that were equilibrated separately in reaction buffer; whereas, previous analyses have involved starting reactions by addition of Mg^{2+} to pre-mixed enzyme and substrate. In addition, differences in reaction conditions, including monovalent ion identity could contribute to these variations in kinetic behavior.

Given that the steady-state kinetic parameters rarely are a direct reflection of enzyme catalytic rate and substrate affinity,[41,42] we examined the multiple turnover reaction kinetics more closely. We noted that plots of product accumulation *versus* time did not extrapolate back to the origin (Figure 2(b)). This behavior suggests that a burst of product formation precedes the steady-state accumulation of product, which would indicate that slow steps after a single round of binding and cleavage are responsible for the linear portion of the reaction. Accordingly, we measured the apparent amplitude of the burst as a function of enzyme concentration. If the burst represents a single round of binding and cleavage, then its amplitude should be proportional to enzyme concentration. The accumulation of products from reactions containing 20 nM RNase III and 100 nM R1.1 RNA, or 40 nM enzyme and 200 nM substrate are shown in Figure 2(b). In both cases the data fit well to a linear equation; however, the lines clearly do not extrapolate to the origin. Importantly, we find that the amplitude of the intercept with the y axis, shown as π in Figure 2(b), increases in direct proportion to enzyme concentration; in all cases, doubling the enzyme concentration doubled the apparent burst amplitude†. Taken together, the relatively slow multiple turnover rate and the presence of a pre-steady-state burst of product formation indicate that a slow step after the first round of binding and cleavage, perhaps product release or an enzyme conformational change, is rate limiting for the multiple turnover reaction.

Pre-steady-state kinetic analysis at low pH

Because the steady-state kinetics do not appear to provide direct information about binding and catalysis, it is essential to define reaction conditions where the apparent reaction rate reflects the rate of substrate cleavage, and where the behavior of active enzyme-substrate complexes can be directly observed. Since hydroxide is presumably the nucleophile in the RNase III catalyzed hydrolysis reaction, lowering the reaction pH should result in a slower catalytic rate, and allow the rate of cleavage of the bound substrate to be determined directly using manual methodology. Figure 3(a) shows that at pH 5.4 the single turnover cleavage rate over a range of enzyme concentrations was slow enough to be determined manually. The data for relatively short reaction times fit well to a single-exponential function; however, longer time-courses are best described by a double-exponential function. At saturating concentrations of enzyme we measure a cleavage rate constant of ca 1 min^{-1} for the fast phase with amplitude of 50-70 % of the total substrate, and a rate constant of ca 0.1 min^{-1} for the slower phase with amplitude of ca 5-10 %. The remaining 20-40 % of the substrate that does not undergo cleavage is presumably in a conformation that is not reactive.

Next, we examined the dependence of the fast phase (k_{obs}) on enzyme concentration (Figure 3(b)). Since these experiments are conducted at enzyme concentrations in excess of substrate, and since the fast cleavage rate is easily isolated by fitting the data to an equation that accounts for the slowly cleaving population, the presence of non-productive, or misfolded RNA substrates should not influence the analysis of pre-steady-state kinetic data. We find that at low concentrations of RNase III (1-35 nM) the single turnover rate is dependent on enzyme concentration, but at higher concentrations the observed rate constant becomes independent of enzyme concentration. This behavior is consistent with a second-order reaction followed by an irreversible first-order reaction, in which the first step is formation of the E-S complex and the second step reflects chemical cleavage as shown in scheme 1:

$$E + S \underset{k_{-1}}{\overset{k_1}{\rightleftharpoons}} E \cdot S \xrightarrow{k_2} E \cdot P$$

Scheme 1

† Assuming the two-step mechanism, $\pi = [E]_0(k_1/(k_1 + k_2))^2$ where k_1 is the apparent first-order rate constant for the single turnover reaction, k_2 is the rate constant for a slow second step that regenerates the free enzyme, and $[E]_0$ is the concentration of enzyme. If all substrates bind productively, and if $k_1 \gg k_2$, then π becomes a measure of active enzyme concentration. We find that the burst amplitudes are ca 40 % of the molar amount of enzyme. However, in single turnover experiments performed at saturating enzyme concentrations a significant fraction (20-30 %) of the substrate is not consumed (see below, Figures 4 and 5), providing evidence for an unreactive population of R1.1 RNAs. In this case the burst amplitude reflects the fraction of bound substrates that are able to undergo cleavage rather than the fraction of enzyme molecules that were active. Thus, 40 % is only a minimum estimate of the fraction of active enzyme.

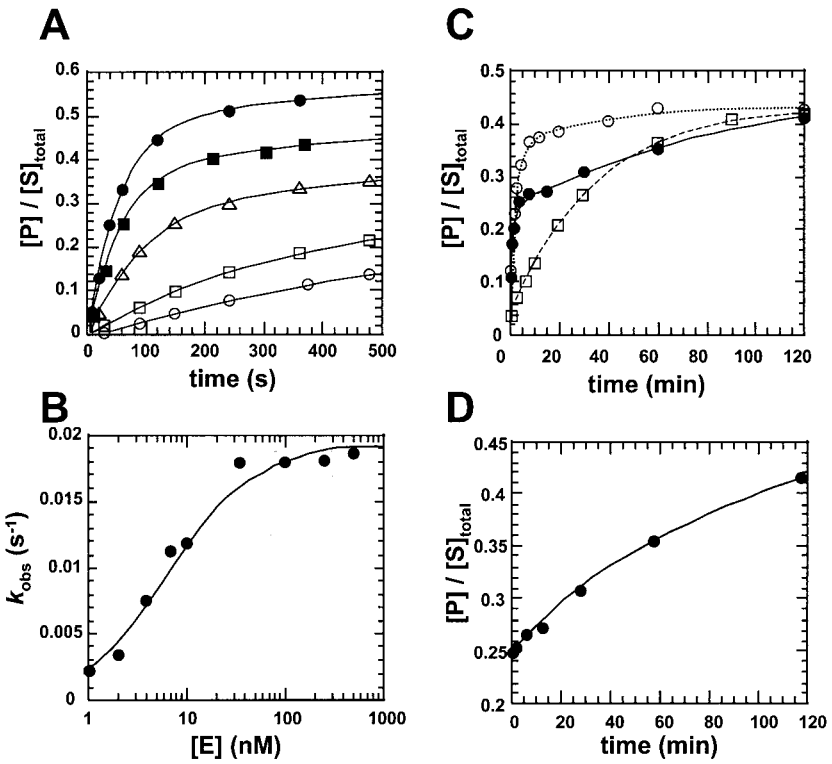

Figure 3. Analysis of pre-steady-state reaction kinetics at low pH. (a) Measurement of single turnover rate constant at low pH. Reactions contain 0.2 nM radiolabeled R1.1 RNA substrate and increasing concentrations of enzyme; open circles, 1 nM; open squares, 2 nM; open triangles, 7 nM; filled squares, 35 nM; and filled circles, 500 nM. The corresponding rates for the predominant fast phase were 0.126 min^{-1}, 0.204 min^{-1}, 0.678 min^{-1}, 1.08 min^{-1} and 1.122 min^{-1}, respectively, determined by fitting the data to a double-exponential equation as described in Materials and Methods. (b) Dependence of the single turnover rate constant on enzyme concentration. The rate constant for the fast phase from single turnover time-courses of R1.1 cleavage (k_{obs}) is plotted *versus* enzyme concentration. The data are fit to a model for a second-order reaction followed by an irreversible first-order reaction as described in the text and in Materials and Methods. The experiment shown here resulted in values for k_2 and K_{app} of 1.158 min^{-1} and 6.08 nM, respectively. The reported values for k_2 and K_{app} ($k_2 = 1.16(\pm0.01)$ min^{-1}; $K_{app} = 5.4(\pm0.6)$ nM) in the text and Table 1 are the average of three independent determinations with standard errors of less than 14 %. (c) Pulse-chase analysis of the relative magnitudes of the rate constants for substrate cleavage (k_2) and dissociation (k_{-1}). Reactions (pH 5.1) contained 2 μM RNase III and 5 nM radiolabeled R1.1 RNA. The fraction of reacted substrate is plotted *versus* time for the reaction that was not chased (open circles); a reaction that was chased with 40 μM cold substrate before mixing enzyme and substrate (open squares); and a reaction that was chased with 40 μM cold substrate at two minutes after initiation of the reaction (filled circles). Data for each reaction are fit to either a single (open squares) or double-exponential function (open and filled circles). (d) Isolated plot of fraction reacted substrate *versus* time for data obtained after the cold chase. Data are fit to a single-exponential function.

In scheme 1, $k_{obs} = [E]k_2/([E] + K_{app})$, where $K_{app} = ((k_2 + k_{-1})/k_1)$. A plot of k_{obs} *versus* enzyme concentration fits well to this mechanism and yields a single turnover rate constant (k_2) at pH 5.4 of 1.16(±0.01) min^{-1} and a K_{app} of 5.4(±0.6) nM (Figure 3(b)).

The parameter K_{app} value is influenced by substrate affinity, as well as the rate of reaction of the enzyme-substrate complex. To examine the extent to which these two aspects of enzyme behavior contribute to K_{app}, we measured the relative rates of substrate dissociation (k_{-1}) and cleavage (k_2) using a pulse-chase approach. First, a population of enzyme-substrate complexes containing radiolabeled RNA was allowed to accumulate prior to addition of an excess of non-radiolabeled substrate. If the rate of substrate dissociation is significantly slower than the rate of cleavage (if $k_2 \gg k_{-1}$), then a chase with cold substrate will have no effect on the rate of product accumulation, since all of the enzyme-substrate complexes formed prior to the chase will go on to form product without dissociating. On the other hand, if the rate of dissociation is faster than cleavage (if $k_2 \ll k_{-1}$), then after the chase, all of the labeled substrate will dissociate and the reaction rate will decrease significantly. Figure 3(c) shows a plot of product accumulation *versus* time for control reactions where either no chase occurred, or the reaction was chased with an excess of cold substrate (40 μM) before mixing enzyme and substrate, and for a reaction that was chased after two minutes. We find that in reactions containing 5 nM radiolabeled substrate, after a chase with 40 μM cold substrate at two minutes the rate of product accumulation decreased rapidly to 0.01 min^{-1} (Figure 3(d)). This rate is very similar to reactions that were ''chased'' before the start of the reaction that yielded a rate constant of 0.02 min^{-1}. Therefore, we conclude that the rate of substrate dissociation is significantly faster (>tenfold) than the rate of cleavage of the bound substrate. Since by definition $K_{app} = ((k_2 + k_{-1})/k_1)$, then if $k_2 \ll k_{-1}$, then K_{app} becomes an approximate measurement of the dissociation constant ($K_d = k_{-1}/k_1$) for substrate binding. As indicated above, we find that K_{app} for the single turnover reaction is 5.4(±0.6) nM, which is similar to the values for K_d measured previously using gel-mobility shift

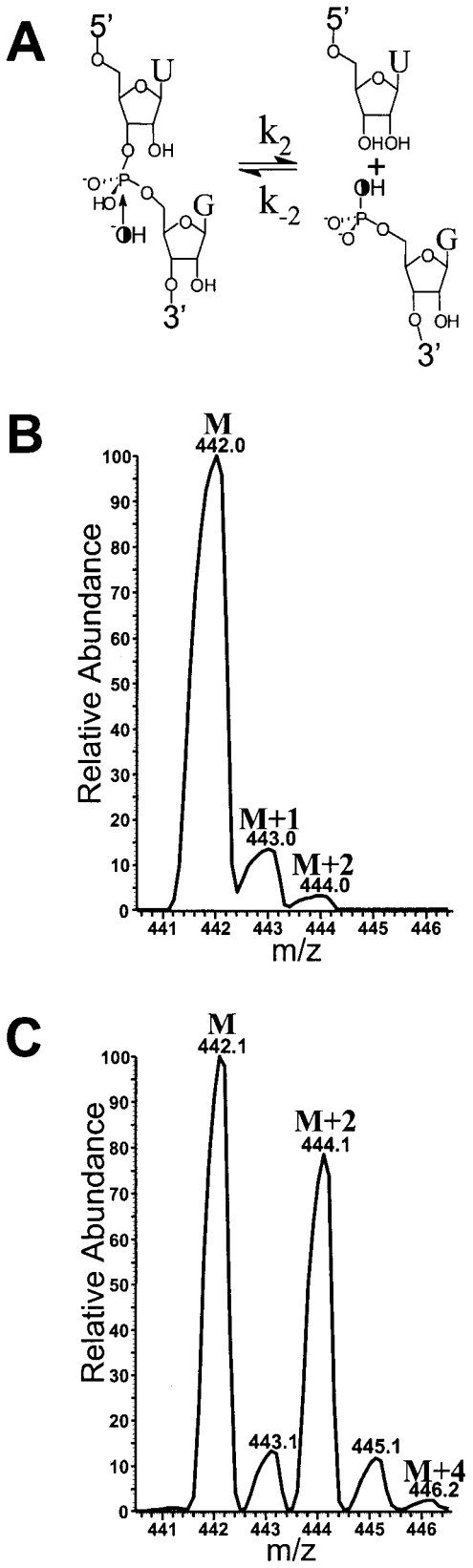

Figure 4. Solvent ^{18}O incorporation during the RNase III reaction. (a) Proposed mechanism for the phosphodiester hydrolysis reaction catalyzed by RNase III. Nucleotides that are 5′ and 3′ to the reactive phosphate are shown. The solvent nucleophile is shown as a half-filled circle. (b) Mass spectrum of enzymatically synthesized control pGp. The value of m/z, or the mass-to-charge ratio, in this experiment is identical with the mass. The monoisotopic mass (442u) is indicated as M and higher molecular mass species due to the presence of natural abundance isotopes are indicated by M + 1 and M + 2. (c) Mass spectrum of pGp containing the reacted phosphate from RNase III cleavage. Reactions were performed under multiple turnover conditions as described in Materials and Methods. The individual species are indicated as in (b). Material due to incorporation of a single ^{18}O at M + 2, as well as a small amount of material at M + 4 (due to natural abundance isotopes) is indicated.

experiments at pH 7.5 ($K_d = 1.8 - 14.4$ nM).[35,43] Thus, the pre-steady-state approach provides a means for measuring both substrate affinity and the rate of cleavage of the bound substrate.

Irreversibility of the cleavage step, and dependence on pH and divalent metal ion identity

Based on the chemistry of non-enzymatic phosphoryl transfer reactions,[44–46] and mechanistic studies of phosphoryl transfer enzymes,[47,48] the RNase III catalyzed reaction almost certainly proceeds in a single step *via* a concerted S_N2 type mechanism. The termini of the products formed by RNase III cleavage of RNA are a 5′ phosphate and a 3′ hydroxyl. Based on these products the mechanism is thought to involve irreversible nucleophilic attack of a solvent water molecule on the phosphate at the cleavage site with the 3′ oxygen atom as the leaving group (Figure 4(a)). However, the chemical details of this mechanism, such as its irreversibility and the incorporation of solvent water have not been tested. Additionally, the concept that enzymes act by stabilization of reaction transition states means that enzymes catalyze both the forward and reverse reactions of a specific chemical transformation. Moreover, it has been argued that enzymes are most efficient when the internal reaction equilibrium is near unity.[49] Thus, although the equilibrium for phosphodiester hydrolysis is expected to lie strongly toward products, in the context of the specialized environment of enzyme active sites this situation may not ensure kinetic irreversibility. In fact, the hydrolysis of ATP to ADP and PO_4^{3-} has been shown to be reversible in ATPases.[50] To gain a better understanding of mechanism and set the stage for subsequent exploration of the catalytic strategies employed by RNase III we employed a simple isotopic incorporation analysis employing ^{18}O-enriched solvent.

A key prediction of the mechanism proposed above is the incorporation of one, and only one, solvent water atom in the newly generated 5′ phosphate on the 3′ cleavage product (Figure 4(a)). To test this prediction we performed the RNase III cleavage reaction in a mixture of $H_2{}^{16}O$ and $H_2{}^{18}O$.

Performing the reaction in ^{18}O-enriched water atom should result in incorporation of a single ^{18}O in the reacted phosphate. Any significant reversal of the reaction will result in the incorporation of additional ^{18}O atoms in the product phosphate upon subsequent re-hydrolysis events. This is because, in the case of reversibility, the free rotation of the 5′ phosphate would allow ^{18}O to be incorporated as a non-bridging oxygen atom in ligated RNA which upon subsequent cleavage results in two ^{18}O atoms in the resulting product. Subsequent to the reaction, the 5′ phosphate of the 3′ cleavage product was purified as the 5′ phosphate of a 3′,5′ guanosine-*bis*-phosphate (pGp) containing the guanosine residue located at the N(+1) position relative to the cleavage site as described in Materials and Methods. The number of ^{18}O atoms incorporated during the hydrolysis reaction was measured by electrospray ionization quadrupole mass spectrometry.

Figure 4(b) shows the mass profile of a control population of pGp derived by treatment of 3′ guanosine monophosphate with polynucleotide kinase and ATP. The major peak at 442u is consistent with the monoisotopic mass of pGp (M). The peak at 443u (M + 1) is due to the presence of natural abundance ^{13}C and ^{15}N. Also, we observe a measurable amount of material at 444u (M + 2), which results from the 0.2 % natural abundance ^{18}O among the 11 oxygen atoms present in pGp. The contrasting mass profile from pGp containing the 5′ phosphate generated in the RNase III cleavage reaction is shown in Figure 4(c). As with the control pGp, a major peak is observed at 442u, and a lesser amount of material with a mass of M + 1 is observed due to natural abundance isotopes. In contrast to the control pGp sample, there is a dramatic increase in the material at M + 2 due to the incorporation of a single ^{18}O atom from solvent during the RNase III catalyzed hydrolysis reaction. Additional material at 445u is due to natural abundance ^{13}C and ^{15}N in the pGp containing the incorporated ^{18}O. Importantly, only background amounts of pGp with mass of M + 4 (compare to M + 2 in Figure 4(b)) are observed that result from the presence of natural abundance levels of ^{18}O in the other ten oxygen atoms in pGp. These results clearly demonstrate that the RNase III catalyzed hydrolysis reaction involves the incorporation of a single ^{18}O atom from solvent, which we interpret as indicating that the reaction is kinetically irreversible.

Any understanding of enzyme catalytic mechanism must necessarily include an examination of the role of proton transfer. Consequently, we explored the extent to which the single turnover rate at saturating enzyme concentration (k_2) is dependent on pH. Figure 5(a) shows a plot of the log of the single turnover rate constant *versus* pH at values between pH 5.1 and pH 6.1. As the pH of the reaction increases the reaction rate also increases, until above pH 6.1 the rate becomes too fast to measure manually. However, it is clear that the reaction

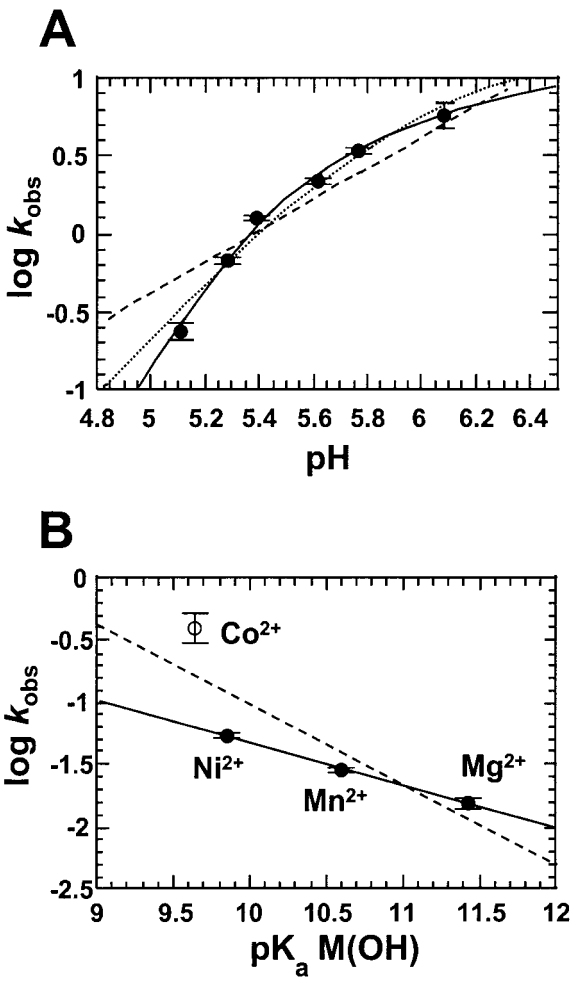

Figure 5. (a) Dependence of the single turnover rate constant on pH. The log of the single turnover rate constant, k_{obs}, is plotted *versus* reaction pH. Each data point is the average of three independent determinations. Error bars represent one standard deviation. The data are fit to models describing the protonation of a single titratable group (broken line), and two or three groups with the same pK_a value (dotted line and continuous line, respectively) as described in the text. Experimental conditions are described in Materials and Methods. (b) Dependence of the single turnover rate constant on metal ion identity. Single turnover assays were performed as described in Materials and Methods. Reactions contained either $MgCl_2$, $MnCl_2$, $NiCl_2$ or $CoCl_2$ at 10 mM. These reactions were performed in MRB at pH 5.4 with 5 nM R1.1 RNA and 2 μM RNase III. The data shown here represent the average of two independent experiments; similar experiments under slightly different buffer conditions yielded similar results. The log of the single turnover rate (k_{obs}) is plotted *versus* the pK_a value of the hydrated form of the metal ion included in the reaction (data from Feig & Uhlenbeck).[56] The error in the value for the rate constant determined in individual experiments with Mg^{2+}, Mn^{2+} and Ni^{2+} was less than 7 %. Reactions containing Co^{2+} were consistently too fast to measure accurately by manual pipetting, and so the rate constants measured in Co^{2+} had errors from 35 to 45 %. Individual data points represent averages and error bars represent one standard deviation. The values for Ni^{2+}, Mn^{2+} and Mg^{2+} fit to a linear equation with a slope of 0.34 (continuous line). A fit of all of the data to a linear equation yielded a line with slope of ca 0.5 (broken line).

rate becomes less dependent on hydroxide concentration at more basic pH values. The simplest model for this behavior is that protonation of a functional group in the enzyme-substrate complex inhibits catalysis:

$$AH \overset{K_a}{\rightleftharpoons} A^- + H^+$$

Scheme 2

where AH is the inactive form of the enzyme, A^- is the active, deprotonated form and the equilibrium between the protonated and deprotonated forms is described by K_a (see Materials and Methods). However, the data fit poorly to an equation describing only a single titratable group in that the rate decreases much more sharply at acidic pH values than predicted (broken line, Figure 5(a)). Next, we considered two titratable groups with differing K_a values:

$$HAH \overset{K_{a1}}{\rightleftharpoons} HA^- + H^+ \overset{K_{a2}}{\rightleftharpoons} A^{2-} + H^+$$

Scheme 3

where HAH and HA^- are inactive, protonated forms and A^{2-} represents the active deprotonated form of the enzyme-substrate complex. A good theoretical fit to the data was obtained with an equation describing this model assuming two different pK_a values for the two titratable groups; however, one of the values was consistently too low to be considered reasonable (p$K_a < 2$). The data also fit well to a similar model assuming that both of the titratable groups have the same pK_a value (p$K_a = 5.9$; dotted line, Figure 5(a)). Interestingly, the best fit was obtained using a variation of this model (see Materials and Methods) that assumed three titratable groups with the same pK_a value (p$K_a = 5.6$; continuous line, Figure 5(a)).

To further explore the relationship between the rate constant k_2 and the substrate cleavage step we determined its dependence on metal ion identity. High-resolution crystal structures of several metal ion dependent phosphodiesterase enzymes, together with chemical and geometric considerations indicate that, in general, a water molecule is activated to carry out nucleophilic attack at the phosphorus atom *via* interactions with divalent metal ions.[27] In these cases, the nucleophile is part of the inner hydration sphere of a metal ion, whereby coordination lowers the pK_a value of the water and therefore increases the concentration of the more nucleophilic metal-hydroxide species.[30,51] If the ability of a metal ion to stimulate catalysis is proportional to the concentration of $M^{2+}(OH^-)$ at the active site, then metal ions with lower pK_a values should have higher cleavage activities due to the increased presence of $M^{2+}(OH^-)$. Thus, an observed relationship between metal ion pK_a values and metal ion cleavage activity has been taken as evidence that a solvated metal hydroxide participates in catalysis.[52]

Accordingly, we determined the single turnover rate constant for reactions conducted in the presence of Mg^{2+}, Mn^{2+}, nickel (Ni^{2+}) and cobalt (Co^{2+}), all of which have been shown to support the RNase III cleavage reaction.[26] As reported previously, two additional metal ions, cadmium (Cd^{2+}) and Ca^{2+}, which were examined as controls, did not support R1.1 cleavage by RNase III (data not shown). Interestingly, the ionic radius of the divalent metal ions that do not support RNase III catalysis are 0.95 Å or greater, whereas the ionic radii of Mg^{2+}, Mn^{2+}, Ni^{2+} and Co^{2+} are all smaller (0.72 Å, 0.67 Å, 0.66 Å and 0.75 Å, respectively), suggesting that there may be a steric limitation on ion size in one or more essential divalent metal ion binding sites in the enzyme-substrate complex.

As shown in Figure 5(b) we find that the pK_a value of the metal ion hydrate correlates with changes in the single turnover rate constant determined with either Mg^{2+}, Mn^{2+}, Ni^{2+} or Co^{2+}. We observe a clear relationship between the log of the single turnover rate constant and the pK_a value of the hydrated divalent metal ion in the reaction; as the metal ion pK_a value decreases, the associated rate constant progressively increases. For Mg^{2+}, Mn^{2+} and Ni^{2+} the data fit very well to a linear equation with a slope of 0.34 (continuous line, Figure 5(b)). Interestingly, reactions performed with Co^{2+} were significantly faster than would be predicted from the relationship between rate and pK_a value for the other metal ions tested; however, the relatively fast rate with Co^{2+} was more difficult to measure precisely. Including the data obtained using Co^{2+} in the linear fit (dotted line, Figure 5(b)) yields a slope of 0.5, but with a significantly poorer fit. Although it is not possible to draw a direct linear relationship for all of the data, there is clearly a correlation between the observed rate in different metal ions and the pK_a value of the metal ion hydrate.

Taken together, the pH dependence of k_2 and the correlation between this kinetic parameter and metal ion identity both suggest that under acidic pH conditions the rate measured at saturating enzyme concentration reflects the chemical step of the reaction. Importantly, we detected no lag in product formation at any of the enzyme concentrations tested, which further supports the conclusion that there are unlikely to be slow steps, such as conformational changes, occurring after binding and before the chemical step. However, kinetic analysis cannot exclude the possibility that changes in enzyme and substrate conformation might occur very rapidly compared with binding and catalysis, or that such changes are in rapid equilibrium relative to these events.

Stopped-flow fluorescence analysis

To examine more closely the possibility that conformational changes were involved in RNase III binding and catalysis, we utilized intrinsic tryptophan fluorescence as a reporter of enzyme confor-

mation in stopped-flow experiments. The RNase III monomer has a single tryptophan residue at 139 that is located between the dsRBD and the catalytic domains of the enzyme; therefore, this residue is not expected to be directly involved in the RNA-protein interface. Thus, any change in intrinsic fluorescence is likely to be due to conformational changes in the protein that alter the environment of Trp139. Single turnover reactions were performed with concentrations of enzyme and substrate that were at least tenfold higher than K_d. Figure 6 shows that following mixing of RNase III with the R1.1 substrate at pH 7.3 in the presence of Mg^{2+} there is a rapid increase in relative fluorescence in the first 0.1 second that is followed by a slower decrease in fluorescence that takes place over a time-scale from zero to one second. Importantly, no change in fluorescence was observed when either enzyme or substrate was mixed with buffer, or when buffer was examined alone (Figure 6, and data not shown). Thus, we conclude that the changes in fluorescence are unlikely to be due to mixing or dilution artifacts, but in fact reflect changes in enzyme conformation occurring during binding and/or catalysis. No other processes were observed over intermediate time-scales (0-60 seconds) (data not shown). Since the apparent pre-steady-state burst observed in multiple turnover experiments takes place in less than ten seconds, we conclude that the rapid increase and slower decrease encompass all of the changes in protein fluorescence that occur during a single round of binding and cleavage by RNase III.

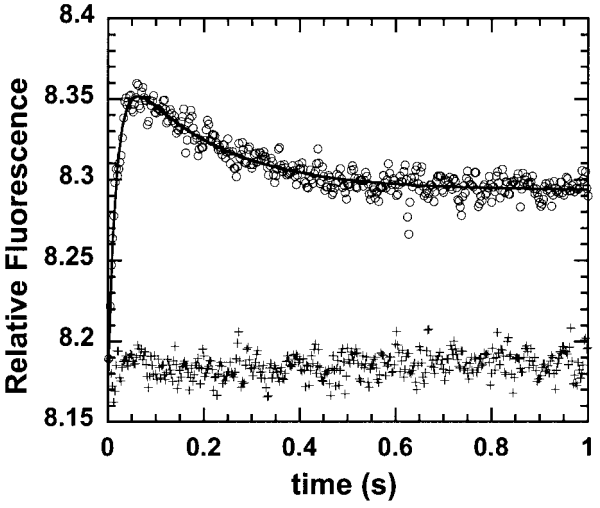

Figure 6. Changes in intrinsic tryptophan fluorescence during the single turnover cleavage of R1.1 RNA by RNase III. Reactions were performed in Tris reaction buffer (pH 7.3) (see Materials and Methods) including 10 mM $MgCl_2$ and contained 1.25 μM RNase III and either 0.8 μM R1.1 RNA (open circles), or buffer solution with no substrate (crosses). The data for the reaction containing substrate are fit to a double-exponential function and the resultant rate constants are reported in Table 1.

Both the fast and slow changes in tryptophan fluorescence fit well to single-exponential functions individually, or a double-exponential function in combination. The fit to a double-exponential function yields a rate constant (k_A) of 55(±5) s^{-1} for the fast phase and a rate constant (k_B) of 6.4(±0.8) s^{-1} for the slow phase at pH 7.3, 10 mM Mg^{2+}, 0.8 μM R1.1 RNA and 1.25 μM RNase III (Table 1). The amplitude of the change in fluorescence is relatively small, which places a constraint on the range of enzyme and substrate concentrations that can be examined, but the fluorescence signal can be readily detected under the single turnover conditions described for Figure 6.

To assess whether the changes in fluorescence were due to bimolecular association of RNase III with the R1.1 substrate or due to unimolecular rearrangements subsequent to binding, we measured k_A and k_B values at a series of substrate concentrations (Figure 7). At concentrations of enzyme and substrate that are greater than tenfold over K_d, a unimolecular rearrangement occurring after substrate binding is not expected to show any significant dependence on the concentration of substrate. On the other hand, conformational changes associated with binding should display concentration dependence. As shown in Figure 7, the fast increase in fluorescence reflected by the rate constant, k_A, is dependent on the concentration of R1.1

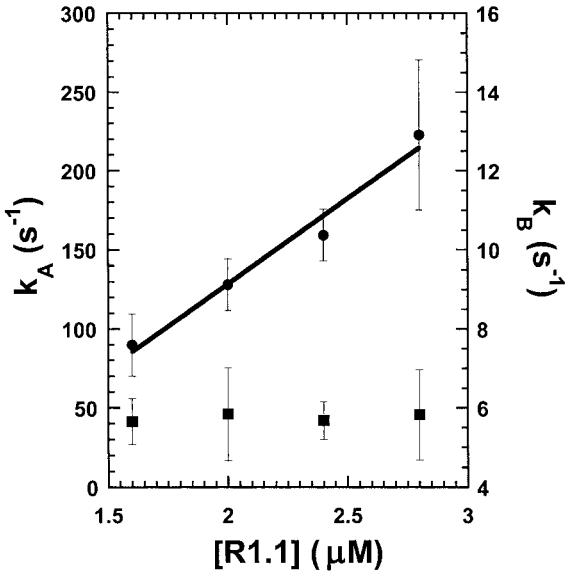

Figure 7. Dependence of k_A and k_B on substrate concentration. Reactions contained 0.25 μM RNase III, a range of R1.1 RNA substrate concentrations, 10 mM $MgCl_2$ and Tris reaction buffer (pH 7.3). Rate constants k_A and k_B were obtained from a fit to a double-exponential function. Rate constants represent the average of at least three experiments with error bars representing one standard deviation. Data for k_A and k_B are depicted by filled circles and squares, respectively. The data for k_A are fit to a linear equation yielding a second-order rate constant of 1.0×10^8 M^{-1} s^{-1}.

Table 1. Effects of pH and divalent metal ion on the single turnover rate constant, k_2, and the rate constants for changes in fluorescence, k_A and k_B

	pH 7.3		pH 6.1	pH 5.8
	Mg^{2+}	Ca^{2+}	Mg^{2+}	Mg^{2+}
k_2 (s^{-1})[a]	n/d	0	0.097 ± 0.016	0.057 ± 0.002
k_A (s^{-1})[b]	55 ± 5	76 ± 7[c]	70 ± 8	52 ± 10
k_B (s^{-1})	6.4 ± 0.8	0	0.17 ± 0.06	0.083 ± 0.007

[a] The single turnover rate constant, k_2, was determined at saturating concentrations of RNase III at pH 6.1 and 5.8 as shown in Figure 5.
[b] Rate constants for both fluorescence transitions, k_A and k_B, were determined using 1.25 μM RNase III and 0.8 μM R1.1 RNA as described in Materials and Methods in the presence of either 10 mM Mg^{2+} or Ca^{2+} as indicated.
[c] Data were fit to a double-exponential equation.

RNA. Fitting these data to a linear equation yields a second-order rate constant of 1×10^8 M^{-1} s^{-1}, suggesting that k_A involves a one-step process associated with binding that occurs 10-100-fold slower than the diffusion controlled limit.[42] In contrast, the subsequent decrease in fluorescence represented by k_B was independent of substrate concentration over the range tested. The lesser magnitude of k_B relative to k_A and its lack of dependence on R1.1 RNA concentration argue that k_B reflects a unimolecular event that occurs subsequent to formation of the enzyme-substrate complex such as catalysis.

To test the hypothesis that k_A is associated with the binding step of the RNase III single turnover reaction and that k_B reflects the cleavage step, we tested their sensitivity to alternative divalent metal ions. It is well established[35] that both binding and cleavage of the R1.1 RNA substrate are dependent on the presence of Mg^{2+}. In contrast, Ca^{2+} clearly supports substrate binding at affinities that are essentially identical with those measured in the presence of Mg^{2+}; however, Ca^{2+} is unable to support catalysis. As shown in Figure 8(a), both fluorescence transitions are observed in reactions containing the optimal divalent metal ion, Mg^{2+}. In contrast, when the stopped-flow fluorescence analysis was carried out with Ca^{2+} only the rapid increase in fluorescence represented by k_A was observed. No subsequent decrease in intrinsic fluorescence was detected, even in reactions monitored for up to one minute (Figure 8(b), and data not shown). Importantly, we find that the rate constant for k_A measured for Ca^{2+} is similar to that determined in the presence of Mg^{2+} ($k_A^{Ca} = 76(\pm 7)$ s^{-1} and $k_A^{Mg} = 55(\pm 5)$ s^{-1}) (Table 1). Additionally, when divalent metal ions were omitted from the reaction, no changes in enzyme fluorescence were detected. The observation that the occurrence of the changes in fluorescence represented by k_A and k_B are dependent on divalent metal ions, and the fact that the second phase (k_B) is observed in the presence of Mg^{2+}, but not Ca^{2+}, provides further support for the conclusion that k_A reflects events associated with substrate binding, while k_B is associated in some manner with catalysis.

In order to test how closely the fluorescence transition represented by k_B corresponds to the rate of substrate cleavage, we examined whether k_B was significantly slower in reactions performed under acidic conditions (pH 5.8 and 6.1; Table 1). As shown in Figure 9(a) and Table 1 there is a significant decrease in k_B as the reaction pH becomes more acidic, similar to the dependence observed for the single turnover catalytic rate. We find that at pH 6.1 there is a ca 40-fold decrease in k_B relative to measurements performed at pH 7.3 ($k_B = 0.17$ s^{-1} (pH 6.1) *versus* $k_B = 6.4$ s^{-1} (pH 7.3)), and an almost 80-fold decrease when the reaction was performed at pH 5.8 ($k_B = 0.083$ s^{-1} (pH 5.8)). In contrast, the rate constant k_A describing the fluorescence transition associated with binding was found to be essentially pH independent with values of ca 55 s^{-1}, 70 s^{-1} and 52 s^{-1} measured at pH 7.3, 6.1 and 5.8, respectively. Thus, the dependence of k_B, and the relative independence of k_A on reaction pH provided additional evidence that these parameters are associated with catalysis and substrate binding, respectively.

A direct comparison between the single turnover catalytic rate constant, k_2, and the fluorescence transition k_B illustrates how closely these two phenomena are coupled (Figure 9(b)). Given the large dependence of both k_2 and k_B on reaction conditions a direct comparison of these rate constants required performing parallel experiments. Thus, essentially identical reaction mixtures of 0.8 μM RNase III and 1.25 μM R1.1 RNA at pH 6.1 were analyzed either by stopped-flow fluorescence, or by product accumulation using a trace amount of radiolabeled RNA. Figure 9(b) shows that the data from both analyses fit single-exponential functions and yield rate constants that are remarkably similar ($k_B = 0.16$ s^{-1} and $k_2 = 0.13$ s^{-1}). Thus, the conformational change reflected by k_B is not only sensitive to pH, as would be expected for a transition associated with RNase III catalysis, but also occurs with a rate constant that is practically indistinguishable from that derived from measuring the accumulation of cleaved RNA product.

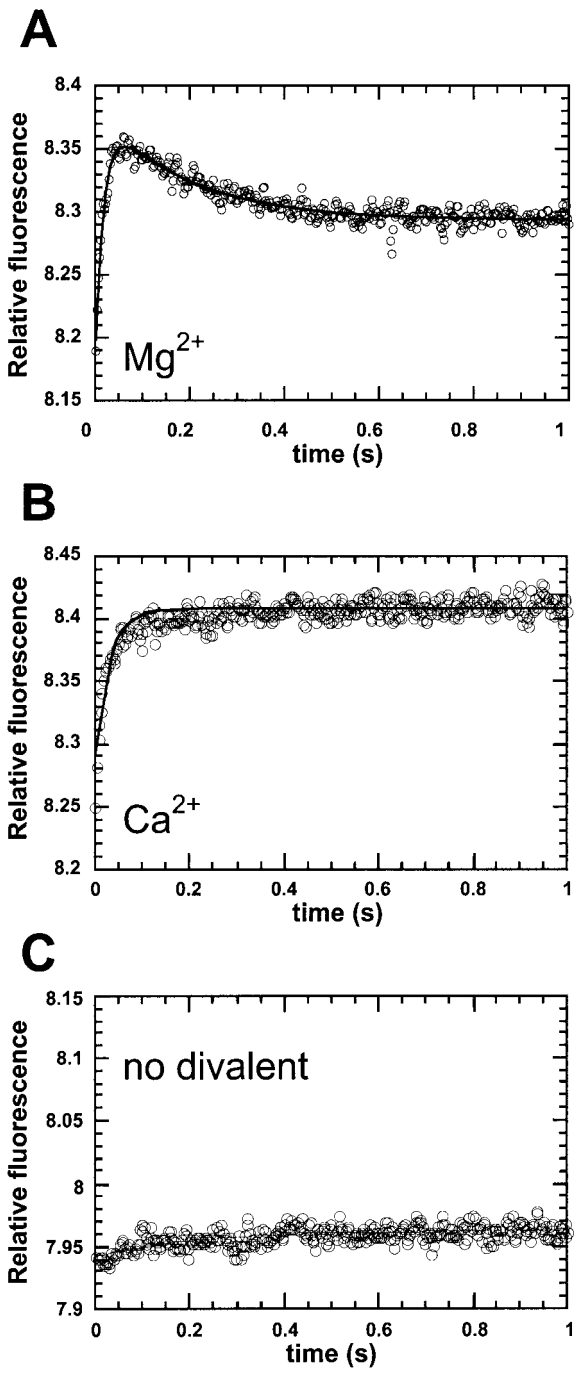

Figure 8. Metal ion dependence of k_A and k_B. Each panel shows the change in intrinsic fluorescence detected in reactions containing 1.25 μM RNase III, 0.8 μM R1.1 RNA, Tris reaction buffer (pH 7.3), and the divalent metal ion indicated. (a) 10 mM $MgCl_2$; (b) 10 mM Ca^{2+}; (c) no metal ion. For the reaction containing Mg^{2+} the data are fit to a double-exponential function, and for reactions containing Ca^{2+} a single-exponential function was used. The resulting rate constants are reported in Table 1.

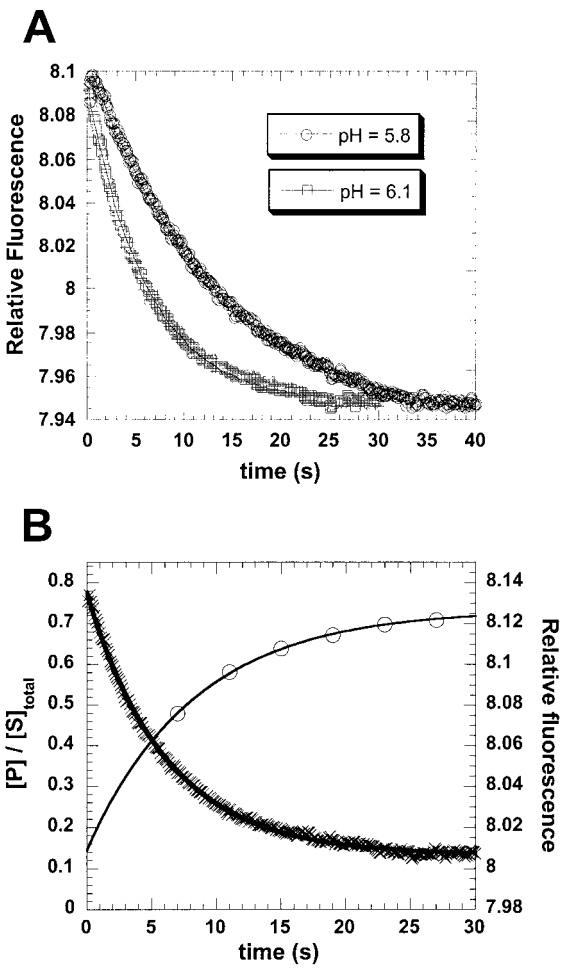

Figure 9. Dependence of k_B on pH. (a) Changes in fluorescence observed in reactions containing 1.25 μM RNase III, 0.8 μM R1.1 RNA, 10 mM $MgCl_2$ and MRB at either pH 5.8 (open circles) or pH 6.1 (open squares). The data are fit to a single-exponential function, since the initial rapid increase in fluorescence is too fast to be observed at this time-scale. Resultant rate constants are listed in Table 1. (b) Correspondence of k_B and the rate constant for product formation determined manually using radiolabeled substrate. Crosses represent fluorescence data obtained at pH 6.1, circles represent data from a parallel reaction that contained identical concentrations of enzyme and substrate, as well as a trace concentration of radiolabeled RNA. The data for both assays are fit to a single-exponential function.

Discussion

These studies allow several conclusions to be drawn concerning the mechanism and reaction kinetics of *E. coli* RNase III cleavage of the R1.1 model substrate. (1) The multiple turnover reaction rate, which has generally been used to assess catalysis by this enzyme, does not directly reflect the rate of cleavage of the bound substrate. (2) At low pH the single turnover rate at saturating enzyme reflects the rate of cleavage of the bound substrate, and

under these conditions substrate association and dissociation are in equilibrium relative to the rate of RNA cleavage. (3) The chemical step is irreversible, involving incorporation of a single solvent oxygen atom during the reaction. (4) The rate of RNA cleavage is sensitive to pH, reflecting a requirement for at least two functional groups in the transition state that can be deprotonated in the accessible pH range. (5) One role of divalent metal ions, which are essential for the catalytic step, is to provide a metal-bound hydroxide that may act as the nucleophile in the hydrolysis reaction. (6) Conformational changes accompany binding and catalysis, and the transition associated with RNA cleavage appears to be concomitant with catalysis. The bases for these deductions are discussed in turn, as well as the implications they have for the function of RNase III.

In general, the multiple turnover cleavage rate has been used to evaluate the effects of mutation, substrate modification and changes in reaction conditions on catalysis by RNase III. However, we find evidence for a pre-steady-state burst of product formation followed by a slower accumulation due to turnover. Additionally, the single turnover rate constant for substrate cleavage at saturating enzyme concentration is faster (ca 6 min^{-1} (pH 6.1); 380 min^{-1} (pH 7.3)) than the relatively slow k_{cat} (1.16 min^{-1} (pH 7.5)). Thus, the rate of product formation during multiple turnover appears to reflect a slow step occurring after catalysis. In this situation, it is difficult to draw straightforward conclusions from structure-function studies based on multiple turnover kinetics, since V_{max} and K_m values under these conditions are dependent on the rate constant for the rate determining step, and do not directly reflect enzyme binding or catalysis. None of the studies presented here directly addresses exactly what step after substrate cleavage is rate limiting for the multiple turnover reaction. It may be that slow release of product, or enzyme isomerization, limits the steady-state cleavage rate, given that conformational changes clearly occur during the reaction. In order to better understand this issue it will be necessary to examine in detail the pathway for dissociation of the two RNA products and measure the extent to which the enzyme is susceptible to product inhibition. Given that substrate dissociation appears to be fast (>10 min^{-1})† relative to the k_{cat}, it is likely that product dissociation might also be similarly fast. Therefore, we hypothesize that an enzyme conformational change, either before or after product dissociation, is rate limiting for multiple turnover. Thus, because of the limitations of the multiple turnover kinetics, it appears from the data presented here that a clear understanding of the mechanisms of RNase III catalysis is best gained from analysis of pre-steady-state kinetics.

The ability to monitor the rate of cleavage of the bound substrate at low pH permitted several basic features of the RNase III catalyzed RNA cleavage reaction to be defined. We find that protonation of two or more functional groups in the enzyme-substrate complex results in inhibition of catalysis. Interestingly, a highly conserved feature of the catalytic domain of RNase III is the presence of several acidic residues. Thus, it is tempting to speculate that one or more of these conserved amino acid residues are involved in the sensitivity of the cleavage reaction to decreasing pH‡. What then, might be the role of these functional groups whose participation in catalysis depends on deprotonation? The proposed mechanism of RNase III hydrolysis involves deprotonation of water to yield the hydroxide ion nucleophile, and protonation of the 3′ oxygen atom leaving group. Thus, it might be expected that protonation of a single functional group (involved in nucleophilic activation) would inhibit catalysis; however, models that invoke two or more basic functional groups best describe the data. A similar sensitivity to pH involving ionization of two carboxylic acid residues involved in nucleophilic activation is observed in the DNA endonuclease *Eco*RV.[54] It is proposed that the proximity of the two carboxylates results in an increase in the ability of one of these residues to accept a proton from the nucleophile. The preponderance of carboxylate residues in the active sites of other phosphodiesterases suggests that this mechanism may be general; however, a second important role for these residues that would also be sensitive to protonation is coordination of active site metal ions.[30,55] In this scenario the inhibition of enzyme activity at low pH would be due to weakened metal ion interactions rather than an inability to perform proton transfer. It may be possible to distinguish between these alternatives by employing the pre-steady-state approaches described here to examine the metal ion dependence of the reaction rate under different pH conditions.

While it is well established that RNase III requires divalent metal ions for activity, the roles of metal ions in catalysis remain undefined. Generally, it is accepted that metal ions play a direct role in catalysis by RNase III similar to other divalent metal ion dependent phosphodiesterases such as restriction enzymes, RNase H, and large ribozymes.[27] One proposed role for metal ions in

† Based on the pulse-chase experiment presented in Figure 3, the rate of substrate dissociation is estimated to be at least tenfold faster than the rate of reaction of the enzyme-substrate complex. Under the conditions used in the pulse-chase analysis the single turnover rate was ca 1 min^{-1} indicating a lower limit for the substrate dissociation rate of ca 10 min^{-1}.

‡ Here the conserved glutamate and aspartate residues in RNase III are given the conventional designation as acidic, although in practical terms their contribution is usually that of Brønsted bases, that is, in their ability to accept a proton at neutral pH. Thus, if the contribution of the conserved glutamate and aspartate residues is to act as anions, then protonation will engender inhibition.[53]

catalysis by this class of enzymes involves interaction with the nucleophile, which serves to lower the pK_a value, thereby resulting in a higher fractionation to hydroxide for the bound water at neutral pH.[51] Intriguingly, we find that the presence of hydrated metal ions with pK_a values lower than that of Mg^{2+} results in a higher catalytic rate, and that there is a significant correlation between the log of the single turnover rate constant and metal ion pK_a. The lower the pK_a value of an individual divalent ion, the greater the fraction of the hydrated ion that will be in the form of metal hydroxide at a given pH. If the ability of a metal ion to stimulate catalysis is proportional to the concentration of metal hydroxide in the active site, then metal ions with lower pK_a values will have higher cleavage rates.[52] The observation of faster RNase III catalytic rates in metal hydrates of decreasing pK_a values argues that a metal ion hydroxide is required for catalysis by this enzyme.

One attractive hypothetical role for this metal hydroxide is in generating the hydroxide ion that is incorporated as the nucleophile in the hydrolysis reaction. Given the correlation between reaction rate and metal ion pK_a it is interesting to note that the slope of a linear fit to the data is less than 1 ($m = 0.34$-0.5). The most general interpretation is that the ability of metal ion hydrate to stimulate the reaction does not depend merely on concentration, in which case the expected slope would be unity. A smaller dependence on pK_a is expected if the activating metal ion hydrate is acting as the nucleophile in the reaction because there is a significant although not absolute dependence of phosphodiester hydrolysis reactions on the basicity of the nucleophile ($\beta_{nuc} = 0.3$).[44] Thus, the rate enhancement from an increase in concentration of the metal-bound hydroxide is partially offset by its decreased reactivity relative to free hydroxide, which has a higher pK_a value.[51] An alternative possibility is that a metal ion hydrate is important for formation of structure in the enzyme substrate complex. Given the importance of metal ion interactions to RNA structure,[56] and evidence of metal ion interactions in the R1.1 RNA internal bulge and loop,[57] it may be that a hydrated metal ion, binding in the deprotonated form to the enzyme-substrate complex, makes a significant contribution to catalysis. This alternative seems less likely, since a much greater dependence on pK_a ($m =$ ca 1) than is observed ($m = 0.34$-0.5; Figure 5(b)) would be expected, as all of the effect on reaction rate would come from the increase in metal hydroxide concentration. Based on these arguments and information from orthologous enzymes, our current model of the chemical reaction includes a metal ion hydroxide as the reactive nucleophile.

The mechanism of the RNase III catalyzed hydrolysis reaction is thought to be S_N2 with the 3′ oxygen atom as the leaving group and a solvent water molecule or hydroxide acting as the nucleophile. This perspective is based on analysis of non-enzymatic phosphodiester hydrolysis reactions using both structure-function relationships,[44] and heavy-atom isotope effects,[46] which demonstrate that phosphodiester hydrolysis reactions are always concerted. Additionally, analysis of the stereochemistry of catalysis by phosphodiesterases such as restriction enzymes shows that cleavage occurs with inversion of configuration.[58,59] Thus, for these enzymes the reaction occurs in a single step and is irreversible. To test the mechanism and reversibility of the RNase III catalyzed reaction we examined incorporation of solvent $H_2{}^{18}O$ into the products of the reaction. Similar approaches have been particularly useful in investigating the mechanisms of ATPases,[60,61] as well as other phosphoryl transfer enzymes.[62–64] As anticipated, we find that a single ^{18}O atom is incorporated into the newly generated 5′ phosphate. This result is consistent with a single-step irreversible hydrolysis mechanism.

In addition to advancing our understanding of the RNase III mechanism the present study also provides, for the first time, an assessment of conformational changes during substrate binding. Conformational changes appear to be a common aspect of RNA-protein interactions, and stopped-flow fluorescence has been successfully used to study RNA-protein dynamics in several cases,[23,24,65,66] as well as for understanding RNA dynamics.[67–69] We find that there are conformational transitions associated with both binding and catalysis by RNase III (Figure 10). The conclusion that the initial, rapid increase in fluorescence upon mixing enzyme and substrate is associated with substrate binding is based on the concentration dependence of the rate constant of this parameter. In addition, this transition shows a metal ion dependence that is similar to that demonstrated for substrate binding. The concentration dependence of k_A yields a second-order rate constant of 1×10^8 M^{-1} s^{-1}, which is less than the diffusion controlled limit for macromolecular interactions.[42] Similar fluorescence transitions upon formation of RNA-protein complexes occurring at equally fast rates have also been observed in substrate binding by aminoacyl-tRNA synthetases (4×10^7 M^{-1} s^{-1}),[23,24] binding of the restriction enzyme *Eco*RV to its substrate (5×10^7 M^{-1} s^{-1}),[70] binding of the termination factor Rho to RNA

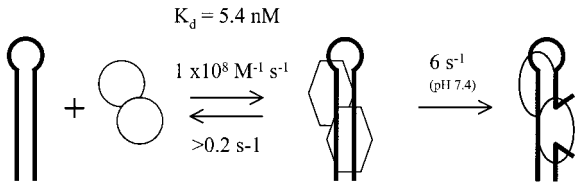

Figure 10. Kinetic scheme for single turnover cleavage of R1.1 RNA by RNase III. The R1.1 RNA is depicted as a stem-loop. RNase III is depicted as gray circles, hexagons or ovals. The changes in enzyme conformation indicated by the changes in fluorescence are depicted using these different shapes.

(8×10^8 M^{-1} s^{-1}),[65] and in the interaction of MS2 coat protein with its cognate RNA stem-loop (2×10^9 M^{-1} s^{-1}).[66] Thus, it seems likely that k_A represents a rapid transition occurring either concomitantly with, or just after the initial interaction between substrate and enzyme (Figure 10).

It is widely assumed that at least part of the interface between RNase III and its substrates involves the dsRBD motif found in all RNase III enzymes. Interestingly, there appears to be few large-scale differences in the three-dimensional structure of the free dsRBD relative to the complexes with RNA.[19,71,72] However, the two available structures show some differences in the RNA-protein interface, making it difficult to predict how the dsRBD is involved in substrate recognition by RNase III. The single tryptophan residue monitored in the experiments described here is located between the conserved catalytic domain of RNase III and the dsRBD. Interdomain linkers, such as those found between the two RNA recognition motifs (RRMs) of U1A and poly(A) binding protein show the greatest change in structure between the free and bound protein.[73,74] Thus, it may be that Trp139 is fortuitously positioned to be a good reporter of inter-domain conformation.

The energetic penalties involved in binding large RNA substrates, which are associated with breaking interactions found in the unbound state, substrate distortion and conformational restrictions, are likely to be significant relative to the positive contribution of binding interactions. The complexities of these issues for interpretation of structure-function studies are illustrated by recent analysis of binding by the well-studied RRM.[37,75] Thus, the observation of conformational changes associated with RNase III substrate binding has a significant implication for structure-function studies of this enzyme. It may be difficult to deconvolute whether changes in the binding equilibrium, due to mutation or modification, result from changes in the structure of the free enzyme or substrate, the bound complex, or some intermediate.

In addition to the rapid increase in fluorescence associated with binding we detect a slower phase that is concomitant with cleavage of the bound substrate (Figure 10). The observation is of interest both because it provides insight into the dynamics of RNase III and because the stopped-flow fluorescence approach provides a convenient continuous assay for both binding and catalytic events. Clearly, combination of this approach with pre-steady-state kinetics using radiolabeled substrate studies will provide a powerful method for exploring molecular recognition and catalysis by RNase III. Interestingly, precedence for the occurrence of conformational changes associated with catalysis within RNA-protein complexes is found in both aminoacyl-tRNA synthetase enzymes[24] and cleavage by the restriction enzyme *Eco*RV.[70] It is of interest to note that similar issues of molecular recognition may be a consideration for RNase III as well. As with most enzymes that interact with RNA or DNA substrates, RNase III has to correctly identify cognate substrates in what has been termed the ''molecular distraction'' of a pool of structurally similar non-cognate RNAs.[76] Obviously, errors in recognition by cellular DNase and RNase enzymes would have ruinous consequences for cell function. One attractive hypothesis is that the conformational changes observed here are relevant to the central issue of how RNase III recognizes structurally diverse substrates.

Materials and Methods

Overexpression, purification and quantification of *E. coli* RNase III

RNase III was overexpressed in HMS174(DE3)/pET11a-RNC cells and purified based on previously described protocols.[26,38,39] Induction of expression resulted in synthesis and accumulation of the 26 kDa RNase III monomer polypeptide. After cell lysis, RNase III was isolated as inclusion bodies, which were washed and subsequently solubilized in a solution containing 8 % (w/v) ammonium sulfate. This material was applied to a column of AG poly(I)-poly(C) agarose (Amersham Pharmacia Biotech) (5 ml bed volume, 2.8 cm × 1.5 cm) equilibrated in buffer containing 0.5 M NH_4Cl. The column was washed with 1 M NH_4Cl, and RNase III was eluted with 2 M NH_4Cl. During chromatography, absorbance of the eluate was monitored at 280 nm. Individual fractions were analyzed by SDS-PAGE, and the RNase III-containing fractions were pooled. SDS-PAGE was carried out using 12 % (w/v) polyacrylamide gels according to standard methods.[77] The gel was stained with Biosafe Coomassie G250 (BioRad), destained with water and air dried between cellophane sheets. The pooled fractions were concentrated twofold in Slide-A-Lyzer 7000 MWCO cassettes (Pierce) by brief exposure to Slide-A-Lyzer Concentrating Solution (Pierce), and were subsequently dialyzed against enzyme storage buffer, ESB (50 % (v/v) glycerol, 0.5 M KCl, 30 mM Tris-HCl (pH 8.0), 0.1 mM EDTA, 0.1 mM DTT) in the same cassettes. The final material was stored in aliquots at −20 °C. Six grams of cells yielded 11 mg of RNase III that was >95 % pure as judged by Coomassie G250 staining of an overloaded SDS-PAGE lane.

The concentration of RNase III was determined using a calculated molar extinction coefficient based on the cysteine, tyrosine and tryptophan content of *E. coli* RNase III.[78,79] The calculated molar extinction coefficient at 280 nm is 13,490 M^{-1} cm^{-1} ($A_{1\%} = 5.3$) for the RNase III monomer (26,980 M^{-1} cm^{-1} for the dimer). This value differs by 2.4-fold from the extinction coefficient reported previously;[26] however, the procedure used to measure this value has not been well described. Since calculated molar extinction coefficients have generally proven to be reliable, even when at odds with measured values,[79] the value of 26,980 M^{-1} cm^{-1} was employed.

For analytical gel filtration chromatography, a Superdex 75 (Amersham Pharmacia Biotech) gel filtration column (129 ml bed volume, 64.5 cm × 1.6 cm) was employed. The separation properties of the column were determined by calibration with proteins of known molecular mass. Specifically, aprotinin (6500 Da), cytochrome *c* (12,400 Da), carbonic anhydrase (29,000 Da), and bovine serum albumin (66,000 Da) were utilized as molecular mass standards and blue dextran

(2,000,000 Da) as a marker for the void volume (V_0). The column was equilibrated in 50 mM Tris-HCl (pH 8.0), 150 mM KCl at a flow rate of 0.5 ml/minute. The markers were dissolved in the same buffer including 5% glycerol and applied to the column in a volume of 1 ml at the same flow rate. Elution of the protein standards was followed by monitoring absorbance at 280 nm. The elution volume (V_e) for each protein was measured and used to calculate a standard curve (molecular mass *versus* V_e/V_0). The apparent molecular mass of RNase III, as well as predicted elution volumes for the dimeric and monomeric forms of the enzyme presented in Figure 1(b) were calculated from the standard curve. For analytical runs, 400 μg of RNase III in 0.1 ml of ESB was applied to the Superdex 75 column that had been equilibrated in a buffer equivalent to ESB but with 5% glycerol instead of 50% glycerol.

Synthesis and purification of RNA

PCR was utilized to create a DNA fragment containing a T7 promoter upstream of the R1.1 RNA coding sequence suitable for cloning into a plasmid vector. The fragment also contained a unique *Bbs*I site so that transcription by T7 RNA polymerase from a plasmid linearized at the *Bbs*I site would yield the R1.1 RNA. Specifically, T7R1.1 (5′ AAGAAGGTCA ATCATAAAGG CCACTCTTGC GAATGACCTT GAGTTTGTCC CTC TACTCCC TATAGTGAGT CGTATTA 3′), which encodes the coding strand of the T7 promoter upstream of the sequence complementary to the R1.1 RNA, was used as the template for PCR using the following primers: R1.1EcoT7For (5′ CGGAATTCTA ATACGACTCA CTATAGGG 3′), and R1.1BbsBamRev (5′ CGGGATCC-GA AGACCGAAGA AGGTCAATCA TAAAGGCC 3′). Oligodeoxyribonucleotides were obtained from Oligos, Etc. A 100 μl PCR reaction containing 1 pmol of T7R1.1 and 100 pmol each of R1.1EcoT7For and R1.1BbsBamRev was used to generate sufficient DNA for cloning. Platinum pfx DNA polymerase (Gibco-BRL) was used in the reaction according to the manufacturer's instructions. The 101 bp double-stranded PCR product was purified from a 2% TAE agarose gel and digested with *Eco*RI and *Bam*HI (New England Biolabs), which cut at each end of the PCR product. The resulting fragment was ligated into similarly cut pUC18, and used to transform the DH5α strain of *E. coli* (Gibco-BRL). Clones were isolated, screened by restriction digest and sequenced using standard molecular cloning procedures,[77] to generate the pT7R1.1 plasmid for *in vitro* transcription of the R1.1 RNA substrate.

R1.1 RNA was synthesized by T7 RNA polymerase as run off transcripts from pT7R1.1 that was linearized by digestion with *Bbs*I (pT7R1.1/*Bbs*I). The product was a 60 nt RNA molecule with the sequence: 5′ GGGAGUA-GAG GGACAAACUC AAGGUCAUUC GCAAGA-GUGG CCUUUAUGAU UGACCUUCUU 3′. *In vitro* transcription reactions contained T7 RNA polymerase transcription buffer (Ambion), 16 mM $MgCl_2$, 5 mM each ATP, CTP, UTP, GTP (Promega), 10 μg pT7R1.1/*Bbs*I, 160 units of Superasin (Ambion), 100 units of yeast inorganic pyrophosphatase (Sigma) and 400 units T7 RNA polymerase (Ambion) in a volume of 400 μl. Transcription reactions were incubated overnight at 37 °C in a dry incubator. Reactions were phenol/chloroform-extracted and RNA was precipitated in the presence of 0.3 M sodium acetate and ethanol. The RNA was recovered by centrifugation, dried, and resuspended in 15 μl of TE (10 mM Tris-HCl (pH 8.0), 1 mM EDTA). In preparation for gel purification, 15 μl of formamide gel loading buffer, GLB (96% (v/v) formamide, 10 mM EDTA, 20 mM Tris-HCl (pH 8.0), 0.025% (w/v) xylene cyanol and 0.025% (w/v) bromophenol blue), was added. The RNA was electrophoresed through a 15% (w/v) polyacrylamide 7 M urea gel, visualized by UV shadowing, excised, and eluted overnight in RNA elution buffer (0.3 M sodium acetate, 0.5% (w/v) SDS, 10 mM Tris-HCl (pH 8.0), 1 mM EDTA). The eluted RNA was extracted twice with phenol/chloroform, once with chloroform, and precipitated with ethanol. After centrifugation, the RNA pellet was washed twice with 80% (v/v) ethanol, air dried, and resuspended in TE. The concentration was determined by measuring absorbance at 260 nm. This protocol routinely resulted in yields of 10-20 nmol R1.1. For larger-scale synthesis, multiple 400 μl reactions were employed. To prepare substrate RNAs for (5′ ^{32}P) end-labeling the transcription reactions were primed with guanosine. Guanosine-primed RNAs were generated using the conditions described above, but with the following changes: 1 mM each ATP, CTP, UTP and GTP, 6 mM guanosine were used. Also, supplemental addition of $MgCl_2$ was omitted.

To prepare (5′-^{32}P) end-labeled R1.1 RNA, 200 pmol of guanosine-primed R1.1 RNA was incubated at 37 °C for one hour in a reaction containing 1 × polynucleotide kinase buffer (New England Biolabs), 400 pmol of [γ-^{32}P]ATP (ICN, end-labeling grade), 100 units of Superasin, and 80 units of T4 polynucleotide kinase (New England Biolabs) in a total volume of 200 μl. The RNA was processed and gel purified as described above except that visualization was by autoradiography. To prepare uniformly ^{32}P-labeled R1.1 RNA, transcription reactions (100 μ) contained 1× transcription buffer, 1 mM each ATP, CTP, and GTP, 0.1 mM UTP, 100 μCi [α-^{32}P]UTP (ICN), 2.5 μg pT7R1.1/BbsI, 40 units Superasin, 25 units of yeast pyrophosphatase and 100 units of T7 RNA polymerase. Reactions were incubated for four hours at 37 °C in a dry incubator. RNA was gel-purified, processed, and quantified as described above. RNA was visualized by autoradiography.

Partial alkaline hydrolysis reactions to generate gel markers contained 25 μg of yeast tRNA (Gibco), 5 μl 0.5 M carbonate buffer (pH 9.5) and (5′-^{32}P) end-labeled RNA in a total volume of 50 μl. The reaction was incubated at 95 °C for five minutes (empirically optimized), chilled on ice, then neutralized with 16 μl of 0.2 M HCl, and an equal volume of formamide GLB was added. Partial ribonuclease T_1 digestion reactions contained 5 μg of yeast tRNA, 10 μl of T_1 buffer (20 mM sodium acetate buffer (pH 5), 7 M urea, 1 mM EDTA), (5′-^{32}P) end-labeled RNA, and 30 units of ribonuclease T_1 (Roche) in a volume of 14 μl. The reaction was incubated for 15 minutes at 50 °C (empirically optimized) and quenched by the addition of 14 μl of ATA stop mix (formamide GLB/100 mM aurin tricarboxylic acid, 4:1).

Analysis of RNase III reaction kinetics

Reactions contained RNase III and R1.1 RNA at the concentrations indicated in the Figure legends and typically in a final reaction volume of 50 μl. Substrate and enzyme solutions were prepared separately. The substrate solutions were prepared in Mes reaction buffer (MRB; 50 mM Mes (Calbiochem) (pH as indicated in the Figure legends), 0.1 mM DTT, 0.1 mM EDTA, 0.01% (v/v) NP40 and 194 mM KCl) and substrate RNA at twice the desired final concentration. The substrate solution

was heated to 95 °C for three minutes and cooled to 37 °C over five minutes. After an additional five minutes at 37 °C, 50 mM $MgCl_2$ in 1 × MRB (preheated to 37 °C) was added to give a final concentration of 10 mM $MgCl_2$ and a final volume of 25 μl. This solution was incubated for an additional 20-60 minutes at 37 °C prior to initiating the reaction. Enzyme solutions were composed of 1 × MRB, 10 mM $MgCl_2$ and twice the final enzyme concentration desired for individual reactions. Enzyme dilutions were made in ESB. Enzyme solution volumes were 25 μl. The stock enzyme solution contributed no more than 10 % of this volume and ESB was added to control for differences in volume of enzyme added. The enzyme solution was preheated for five minutes at 37 °C prior to initiating the reaction. Reactions were initiated by adding an equal volume (usually 25 μl) of substrate solution to the enzyme solution and mixed rapidly using gentle pipetting. At each desired time-point, a 2 μl aliquot was removed from the reaction and added to a tube containing 4 μl of formamide GLB containing 100 mM EDTA. The samples were loaded directly on a 15 % polyacrylamide 7 M urea gel and electrophoresis continued until the bromophenol blue dye reached the bottom of the gel. Gels were dried and RNA bands were quantified by phosphorimager analysis using Molecular Dynamics screens and instrumentation and using ImageQuant software.

The dependence of the single turnover rate constant on enzyme concentration was determined as follows. Reactions were performed as described above in MRB (pH 5.4), 10 mM $MgCl_2$, 0.2 nM R1.1 substrate and 1 nM to 2 μM RNase III ([E]/[S] ⩾ 5). For each enzyme concentration, the fraction of substrate reacted was quantified at each time-point, and these data were displayed as a plot of the fraction of the total substrate reacted *versus* time. The data were fit to a double-exponential function:

$$[P]/[S]_{total} = A - (Be_{\alpha}^{-k}(t) + Ce_{\beta}^{-k}(t)) \quad (1)$$

where A represents the reaction endpoint, B and C represent amplitudes of the two phases, k_α and k_β represent the rate constants of the two phases, and t is the time of incubation. The value for the fast phase, k_{obs}, was plotted *versus* enzyme concentration and the data points are fit to equation (2) (see Results):

$$k_{obs} = [E]k_2/([E] + K_{app}) \quad (2)$$

where k_{obs} is the observed pseudo-first-order rate constant, [E] is the enzyme concentration, k_2 is the cleavage rate constant at saturating enzyme concentration and $K_{app} = ((k_2 + k_{-1})/k_1)$ according to Scheme 1. The reported values for k_2 and K_{app} are the average of three determinations.

Pulse-chase experiments were performed as described above in MRB (pH 5.1) and 10 mM $MgCl_2$, with 5 nM (5′-^{32}P) end-labeled R1.1 substrate and 2 μM RNase III. Reactions were chased after two minutes with the addition of excess, unlabeled R1.1 RNA (40 μM) that was prepared in parallel with labeled RNA substrate. Parallel control reactions were carried out without a chase, and with the chase added at the start of the reaction. Products were quantified and the data analyzed as described above.

The dependence of the single turnover rate constant on pH was determined using 5 nM R1.1 substrate and 2 μM RNase III as described above. The reaction rate at saturating enzyme was measured at six different pH values: 5.1, 5.3, 5.4, 5.6, 5.8, and 6.1. In all cases, the pH reported is the pH of the final reaction mixture taken at 37 °C. Buffers for determination of the pH dependence of the single turnover rate were generated as follows. Sufficient components of 3 × Mes core solution (240 mM KCl, 150 mM Mes, 0.3 mM DTT, 0.3 mM EDTA) were combined for a final solution volume of 280 ml; however, the working volume prior to adjusting pH was maintained at 200 ml. The pH values of aliquots of this solution were adjusted, at room temperature, through measured additions of 10 M KOH, to give a range of pH values from pH 5 to pH 6.5. Since the K^+ concentration in each solution varied, KCl was added to normalize the K^+ concentration to reach a concentration of 114 mM. Solutions were filtered through 0.2 μm filters and stored at −20 °C. Each 3 × Mes solution (corresponding to different pH values) was used to create a 30 ml mock reaction that was identical with actual reactions except that enzyme storage buffer was used in place of enzyme. Each mock reaction was equilibrated at 37 °C, and its pH determined to give the final pH of the reaction.

The following equations were used to fit the pH dependence of the RNase III cleavage reaction.[42] For a single ionizable group the observed rate constant is expected to vary with pH as described by:

$$k_{obs} = \frac{k_A}{1 - 10^{(pK_a - pH)}} \quad (3)$$

where k_{obs} is the observed rate constant at a particular pH, k_A is the activity of the deprotonated species and it is assumed that protonated species are inactive. For systems with two or more ionizable groups the following equation was used:

$$k_{obs} = \frac{k_A}{1 + n(10^{(pK_a - pH)}) + (10^{(pK_a - pH)})^n} \quad (4)$$

where k_{obs} is the observed rate constant at a particular pH, k_A is the activity of the deprotonated species and n is the number of ionizable groups with the same pK_a.

Isotope incorporation measurements

Isotope incorporation reactions were performed in MRB (pH 5.1) including 10 mM $MgCl_2$. The reactions contained 150 μM R1.1 substrate and 5 μM RNase III in a volume of 200 μl, and were incubated overnight at 37 °C. The ^{18}O content of the water was enriched to ∼40 % using 97 %+ ^{18}O water (Isotec). The reacted phosphate was purified in the form of 5′,3′-guanosine-*bis*-phosphate (pGp) as follows. The 3′ product of the reaction was purified using denaturing PAGE, eluted and precipitated as described above. The recovered product was digested to mononucleotides with RNase T_2 (Sigma). The pGp containing the reactive phosphate was purified away from nucleotide monophosphates by HPLC using a C_{18} reverse phase column (Phenomenex) run isocratically in 50 mM diisoprolyethylamine and 1 % (v/v) acetic acid (pH 4.3). The fractions containing pGp were desalted using multiple rounds of lyophilization and resuspension in water. For mass spectrometric analysis, pGp was resuspended in a mixture of water methanol and acetic acid (50:50:1, by volume) at a concentration of 100 μM. Mass spectra were taken using a Finnigan TSQ quadrupole mass spectrometer with an electrospray ion source. Standard pGp was synthesized by treating 3′-guanosine monophosphate with polynucleotide kinase and ATP and purified as described above.

Stopped-flow fluorescence analysis

Fluorescence analysis was performed on an Applied Photophysics π* 180 spectrometer. Reactions were performed in MRB (pH 5.8 or 6.1) or Tris reaction buffer (MRB, but with 30 mM Tris-HCl (pH 7.3) in place of Mes and 80 mM KCl). Reactions additionally contained (10 mM) the indicated metal ion chloride. Temperature was regulated at 37.0(±0.1) °C using a circulating water bath. Reactions were initiated by injecting equal volumes of substrate and enzyme into a flow cell. Concentrations given for RNase III and R1.1 are the concentrations after mixing. Excitation at 290 nm was performed using a variable wavelength monochromator and a 75 W mercury-xenon lamp. Fluorescence emission was detected at 90 ° using a 320 nm cut-off filter. The fluorescence time-courses shown are the average of between two and six individual time-courses. Data exhibiting single-phase behavior were fit to a single-exponential equation function:

$$y = \mathrm{A} - B\mathrm{e}^{-k(t)} \quad (5)$$

where y is the relative fluorescence, A is the reaction endpoint, B represents the amplitude, k represents the exponential rate constant and t is the time after injection. Data exhibiting biphasic behavior were fit to a double-exponential function according to equation (1), above.

Acknowledgments

We thank Dr Mark Caprara, Dr Pieter deHaseth and the members of the Harris laboratory for advice and critical reading of the manuscript. We gratefully acknowledge the assistance of Stephen Ingalls for mass spectrometric analysis. We thank Dr Allen W. Nicholson for generously providing the bacterial strain used in purification of wild-type *E. coli* RNase III. A.G.C. was supported by an HHMI graduate fellowship.

References

1. Robertson, H. D., Webster, R. E. & Zinder, N. D. (1968). Purification and properties of ribonuclease III from *Escherichia coli*. *J. Biol. Chem.* **243**, 82-91.
2. Nicholson, A. W. (1999). Function, mechanism and regulation of bacterial ribonucleases. *FEMS Microbiol. Rev.* **23**, 371-390.
3. Dunn, J. J. & Studier, F. W. (1973). T7 early RNAs and *Escherichia coli* ribosomal RNAs are cut from large precursor RNAs *in vivo* by ribonuclease 3. *Proc. Natl Acad. Sci. USA,* **70**, 3296-3300.
4. Young, R. A. & Steitz, J. A. (1978). Complementary sequences 1700 nucleotides apart form a ribonuclease III cleavage site in *Escherichia coli* ribosomal precursor RNA. *Proc. Natl Acad. Sci. USA,* **75**, 3593-3597.
5. Burgin, A. B., Parodos, K., Lane, D. J. & Pace, N. R. (1990). The excision of intervening sequences from *Salmonella* 23 S ribosomal RNA. *Cell,* **60**, 405-414.
6. Regnier, P. & Grunberg-Manago, M. (1990). RNase III cleavages in non-coding leaders of *Escherichia coli* transcripts control mRNA stability and genetic expression. *Biochimie,* **72**, 825-834.
7. Moller-Jensen, J., Franch, T. & Gerdes, K. (2001). Temporal translational control by a metastable RNA structure. *J. Biol. Chem.* **276**, 35707-35713.
8. Abou Elela, S. & Ares, M., Jr (1998). Depletion of yeast RNase III blocks correct U2 3′ end formation and results in polyadenylated but functional U2 snRNA. *EMBO J.* **17**, 3738-3746.
9. Chanfreau, G., Legrain, P. & Jacquier, A. (1998). Yeast RNase III as a key processing enzyme in small nucleolar RNAs metabolism. *J. Mol. Biol.* **284**, 975-988.
10. Abou Elela, S. A., Igel, H. & Ares, M., Jr. (1996). RNase III cleaves eukaryotic preribosomal RNA at a U3 snoRNP-dependent site. *Cell,* **85**, 115-124.
11. Bernstein, E., Caudy, A. A., Hammond, S. M. & Hannon, G. J. (2001). Role for a bidentate ribonuclease in the initiation step of RNA interference. *Nature,* **409**, 363-366.
12. Kharrat, A., Macias, M. J., Gibson, T. J., Nilges, M. & Pastore, A. (1995). Structure of the dsRNA binding domain of *E. coli* RNase III. *EMBO J.* **14**, 3572-3584.
13. St. Johnston, D., Brown, N. H., Gall, J. G. & Jantsch, M. (1992). A conserved double-stranded RNA-binding domain. *Proc. Natl Acad. Sci. USA,* **89**, 10979-10983.
14. Mian, I. S. (1997). Comparative sequence analysis of ribonucleases HII, III, II PH and D. *Nucl. Acids Res.* **25**, 3187-3195.
15. Chelladurai, B., Li, H., Zhang, K. & Nicholson, A. W. (1993). Mutational analysis of a ribonuclease III processing signal. *Biochemistry,* **32**, 7549-7558.
16. Krinke, L. & Wulff, D. L. (1990). The cleavage specificity of RNase III. *Nucl. Acids Res.* **18**, 4809-4815.
17. Chelladurai, B. S., Li, H. & Nicholson, A. W. (1991). A conserved sequence element in ribonuclease III processing signals is not required for accurate *in vitro* enzymatic cleavage. *Nucl. Acids Res.* **19**, 1759-1766.
18. Zhang, K. & Nicholson, A. W. (1997). Regulation of ribonuclease III processing by double-helical sequence antideterminants. *Proc. Natl Acad. Sci. USA,* **94**, 13437-13441.
19. Perez-Canadillas, J. M. & Varani, G. (2001). Recent advances in RNA-protein recognition. *Curr. Opin. Struct. Biol.* **11**, 53-58.
20. Williamson, J. R. (2000). Induced fit in RNA-protein recognition. *Nature Struct. Biol.* **7**, 834-837.
21. Leulliot, N. & Varani, G. (2001). Current topics in RNA-protein recognition: control of specificity and biological function through induced fit and conformational capture. *Biochemistry,* **40**, 7947-7956.
22. Zheng, X. & Bevilacqua, P. C. (2000). Straightening of bulged RNA by the double-stranded RNA-binding domain from the protein kinase PKR. *Proc. Natl Acad. Sci. USA,* **97**, 14162-14167.
23. Baltzinger, M. & Holler, E. (1982). Kinetics of acyl transfer ribonucleic acid complexes of *Escherichia coli* phenylalanyl-tRNA synthetase. A conformational change is rate limiting in catalysis. *Biochemistry,* **21**, 2460-2467.
24. Ibba, M., Johnson, C. M., Hennecke, H. & Fersht, A. R. (1995). Increased rates of tRNA charging through modification of the enzyme-aminoacyl-adenylate complex of phenylalanyl-tRNA synthetase. *FEBS Letters,* **358**, 293-296.
25. Baldwin, G. S., Sessions, R. B., Erskine, S. G. & Halford, S. E. (1999). DNA cleavage by the EcoRV restriction endonuclease: roles of divalent metal ions in specificity and catalysis. *J. Mol. Biol.* **288**, 87-103.

26. Li, H. L., Chelladurai, B. S., Zhang, K. & Nicholson, A. W. (1993). Ribonuclease III cleavage of a bacteriophage T7 processing signal. Divalent cation specificity, and specific anion effects. *Nucl. Acids Res.* **21**, 1919-1925.
27. Wilcox, D. E. (1996). Binuclear metallohydrolases. *Chem. Rev.* **96**, 2435-2458.
28. Cowan, J. A. (1997). Metal-mediated hydrolysis of biological phosphate esters. *J. Biol. Inorg. Chem.* **2**, 168-176.
29. Steitz, T. A. & Steitz, J. A. (1993). A general two-metal-ion mechanism for catalytic RNA. *Proc. Natl Acad. Sci. USA,* **90**, 6498-6502.
30. Beese, L. S. & Steitz, T. A. (1991). Structural basis for the 3′-5′ exonuclease activity of *Escherichia coli* DNA polymerase I: a two metal ion mechanism. *EMBO J.* **10**, 25-33.
31. Mol, C. D., Kuo, C. F., Thayer, M. M., Cunningham, R. P. & Tainer, J. A. (1995). Structure and function of the multifunctional DNA-repair enzyme exonuclease III. *Nature,* **374**, 381-386.
32. Vipond, I. B., Baldwin, G. S. & Halford, S. E. (1995). Divalent metal ions at the active sites of the EcoRV and EcoRI restriction endonucleases. *Biochemistry,* **34**, 697-704.
33. Shan, S., Yoshida, A., Sun, S., Piccirilli, J. A. & Herschlag, D. (1999). Three metal ions at the active site of the *Tetrahymena* group I ribozyme. *Proc. Natl Acad. Sci. USA,* **96**, 12299-12304.
34. Hosfield, D. J., Guan, Y., Haas, B. J., Cunningham, R. P. & Tainer, J. A. (1999). Structure of the DNA repair enzyme endonuclease IV and its DNA complex: double-nucleotide flipping at abasic sites and three-metal-ion catalysis. *Cell,* **98**, 397-408.
35. Li, H. & Nicholson, A. W. (1996). Defining the enzyme binding domain of a ribonuclease III processing signal. Ethylation interference and hydroxyl radical footprinting using catalytically inactive RNase III mutants. *EMBO J.* **15**, 1421-1433.
36. Sun, W. & Nicholson, A. W. (2001). Mechanism of action of *Escherichia coli* ribonuclease III. Stringent chemical requirement for the glutamic acid 117 side-chain and Mn^{2+} rescue of the Glu117Asp mutant. *Biochemistry,* **40**, 5102-5110.
37. Kranz, J. K. & Hall, K. B. (1998). RNA binding mediates the local cooperativity between the beta-sheet and the C-terminal tail of the human U1A RBD1 protein. *J. Mol. Biol.* **275**, 465-481.
38. Dunn, J. J. (1976). RNase III cleavage of single-stranded RNA. Effect of ionic strength on the fideltiy of cleavage. *J. Biol. Chem.* **251**, 3807-3814.
39. Chen, S. M., Takiff, H. E., Barber, A. M., Dubois, G. C., Bardwell, J. C. & Court, D. L. (1990). Expression and characterization of RNase III and Era proteins. Products of the rnc operon of *Escherichia coli*. *J. Biol. Chem.* **265**, 2888-2895.
40. Nicholson, A. W., Niebling, K. R., McOsker, P. L. & Robertson, H. D. (1988). Accurate *in vitro* cleavage by RNase III of phosphorothioate-substituted RNA processing signals in bacteriophage T7 early mRNA. *Nucl. Acids Res.* **16**, 1577-1591.
41. Northrop, D. B. (1998). On the meaning of K_m and *V/K* in enzyme kinetics. *J. Chem. Ed.* **75**, 1153-1157.
42. Fersht, A. (1998). *Structure and Mechanism in Protein Science*, pp. 155-168, W.H. Freeman & Co., New York.
43. Calin-Jageman, I., Amarasinghe, A. K. & Nicholson, A. W. (2001). Ethidium-dependent uncoupling of substrate binding and cleavage by *Escherichia coli* ribonuclease III. *Nucl. Acids Res.* **29**, 1915-1925.
44. Kirby, A. J. & Younas, M. (1970). The reactivity of phosphate esters. Reactions of diesters with nucleophiles. *J. Chem. Soc. (B),* 1165-1172.
45. Herschlag, D. & Jencks, W. P. (1989). Phosphoryl transfer to anionic oxygen nucleophiles. Nature of the transition state and electrostatic repulsion. *J. Am. Chem. Soc.* **111**, 7587-7596.
46. Hengge, A. C., Aleksandra, T. E. & Cleland, W. W. (1995). Studies of transition-state structures of phosphoryl transfer reactions of phosphodiesters of *p*-nitrophenol. *J. Am. Chem. Soc.* **117**, 5919-5926.
47. Knowles, J. R. (1980). Enzyme-catalyzed phosphoryl transfer reactions. *Annu. Rev. Biochem.* **49**, 877-919.
48. Hengge, A. C. (2001). Isotope effects in the study of enzymatic phosphoryl transfer reactions. *FEBS Letters,* **501**, 99-102.
49. Burbaum, J. J., Raines, R. T., Albery, W. J. & Knowles, J. R. (1989). Evolutionary optimization of the catalytic effectiveness of an enzyme. *Biochemistry,* **28**, 9293-9305.
50. Wu, D. & Boyer, P. D. (1986). Bound adenosine 5′-triphosphate formation, bound adenosine 5′-diphosphate and inorganic phosphate retention, and inorganic phosphate oxygen exchange by chloroplast adenosinetriphosphatase in the presence of Ca^{2+} or Mg^{2+}. *Biochemistry,* **25**, 3390-3396.
51. Herschlag, D. & Jencks, W. P. (1990). Catalysis of the hydrolysis of phosphorylated pyridines by $Mg(OH)+$: a possible model for enzymatic phosphoryl transfer. *Biochemistry,* **29**, 5172-5179.
52. Dahm, S. C., Derrick, W. B. & Uhlenbeck, O. C. (1993). Evidence for the role of solvated metal hydroxide in the hammerhead cleavage mechanism. *Biochemistry,* **32**, 13040-13045.
53. Cornish-Bowden, A. J. (1995). *Fundamentals of Enzyme Kinetics*, pp. 180-181, Portland Press Ltd, London.
54. Stanford, N. P., Halford, S. E. & Baldwin, G. S. (1999). DNA cleavage by the *Eco*RV restriction endonuclease: pH dependence and proton transfers in catalysis. *J. Mol. Biol.* **288**, 105-116.
55. Viadiu, H. & Aggarwal, A. K. (1998). The role of metals in catalysis by the restriction endonuclease *Bam*HI. *Nature Struct. Biol.* **5**, 910-916.
56. Feig, A. L. & Uhlenbeck, O. C. (1999). The role of metal ions in RNA biochemistry. In *The RNA World* (Gesteland, R. F., Cech, T. R. & Atkins, J. F., eds), 2nd edit., pp. 287-320, Cold Spring Harbor Laboratory Press, Cold Spring Harbor, NY.
57. Schweisguth, D. C., Chelladurai, B. S., Nicholson, A. W. & Moore, P. B. (1994). Structural characterization of a ribonuclease III processing signal. *Nucl. Acids Res.* **22**, 604-612.
58. Connolly, B. A., Eckstein, F. & Pingoud, A. (1984). The stereochemical course of the restriction endonuclease *Eco*RI-catalyzed reaction. *J. Biol. Chem.* **259**, 10760-10763.
59. Grasby, J. A. & Connolly, B. A. (1992). Stereochemical outcome of the hydrolysis reaction catalyzed by the *Eco*RV restriction endonuclease. *Biochemistry,* **31**, 7855-7861.
60. Bagshaw, C. R., Trentham, D. R., Wolcott, R. G. & Boyer, P. D. (1975). Oxygen exchange in the gamma-phosphoryl group of protein-bound ATP during Mg^{2+}-dependent adenosine triphosphatase activity of myosin. *Proc. Natl Acad. Sci. USA,* **72**, 2592-2596.

61. Abend, A., Garrison, P. N., Barnes, L. D. & Frey, P. A. (1999). Stereochemical retention of the configuration in the action of Fhit on phosphorus-chiral substrates. *Biochemistry,* **38**, 3668-3676.
62. Cho, Y. K., Matsunaga, T. O., Kenyon, G. L., Bertagnolli, B. L. & Cook, P. F. (1988). Isotope exchange as a probe of the kinetic mechanism of pyrophosphate-dependent phosphofructokinase. *Biochemistry,* **27**, 3320-3325.
63. Zhang, Z. Y., Malachowski, W. P., Van Etten, R. L. & Dixon, J. E. (1994). Nature of the rate-determining steps of the reaction catalyzed by the *Yersinia* protein-tyrosine phosphatase. *J. Biol. Chem.* **269**, 8140-8145.
64. Walker, H., Ferretti, J. A. & Stadtman, T. C. (1998). Isotope exchange studies on the *Escherichia coli* selenophosphate synthetase mechanism. *Proc. Natl Acad. Sci. USA,* **95**, 2180-2185.
65. Kim, D. E. & Patel, S. S. (2001). The kinetic pathway of RNA binding to the *Escherichia coli* transcription termination factor Rho. *J. Biol. Chem.* **276**, 13902-13910.
66. Lago, H., Parrott, A. M., Moss, T., Stonehouse, N. J. & Stockley, P. G. (2001). Probing the kinetics of formation of the bacteriophage MS2 translational operator complex: identification of a protein conformer unable to bind RNA. *J. Mol. Biol.* **305**, 1131-1144.
67. Silverman, S. K. & Cech, T. R. (1999). RNA tertiary folding monitored by fluorescence of covalently attached pyrene. *Biochemistry,* **38**, 14224-14237.
68. Qin, P. Z. & Pyle, A. M. (1997). Stopped-flow fluorescence spectroscopy of a group II intron ribozyme reveals that domain 1 is an independent folding unit with a requirement for specific Mg^{2+} ions in the tertiary structure. *Biochemistry,* **36**, 4718-4730.
69. Bevilacqua, P. C., Li, Y. & Turner, D. H. (1994). Fluorescence-detected stopped flow with a pyrene labeled substrate reveals that guanosine facilitates docking of the 5′ cleavage site into a high free energy binding mode in the *Tetrahymena* ribozyme. *Biochemistry,* **33**, 11340-11348.
70. Baldwin, G. S., Vipond, I. B. & Halford, S. E. (1995). Rapid reaction analysis of the catalytic cycle of the *Eco*RV restriction endonuclease. *Biochemistry,* **34**, 705-714.
71. Bycroft, M., Grunert, S., Murzin, A. G., Proctor, M. & St Johnston, D. (1995). NMR solution structure of a dsRNA binding domain from *Drosophila* Staufen protein reveals homology to the N-terminal domain of ribosomal protein S5. *EMBO J.* **14**, 3563-3571.
72. Ramos, A., Grunert, S., Adams, J., Micklem, D. R., Proctor, M. R., Freund, S. *et al*. (2000). RNA recognition by a Staufen double-stranded RNA-binding domain. *EMBO J.* **19**, 997-1009.
73. Handa, N., Nureki, O., Kurimoto, K., Kim, I., Sakamoto, Y., Muto, Y. & Yokoyama, S. (1999). Structural basis for recognition of the tra mRNA precursor by the Sex-lethal protein. *Nature,* **398**, 579-585.
74. Deo, R. C., Bonanno, J. B., Sonenberg, N. & Burley, S. K. (1999). Recognition of polyadenylate RNA by the poly(A)-binding protein. *Cell,* **98**, 835-845.
75. Reyes, C. M. & Kollman, P. A. (2000). Structure and thermodynamics of RNA-protein binding: using molecular dynamics and free energy analyses to calculate the free energies of binding and conformational change. *J. Mol. Biol.* **297**, 1145-1158.
76. Jen-Jacobson, L. (1997). Protein-DNA recognition complexes: conservation of structure and binding energy in the transition state. *Biopolymers,* **44**, 153-180.
77. Sambrook, J., Fritsh, E. F. & Maniatis, T. (1989). *Molecular Cloning: A Laboratory Manual*, 2nd edit., Cold Spring Harbor Laboratory Press, Cold Spring Harbor, NY.
78. Nashimoto, H. & Uchida, H. (1985). DNA sequencing of the *Escherichia coli* ribonuclease III gene and its mutations. *Mol. Gen. Genet.* **201**, 25-29.
79. Gill, S. C. & von Hippel, P. H. (1989). Calculation of protein extinction coefficients from amino acid sequence data. *Anal. Biochem.* **182**, 319-326.

Edited by J. Karn

(Received 22 October 2001; received in revised form 10 January 2002; accepted 10 January 2002)